1957

Endurance of a full-scale pretensioned concrete member, (Progress Report No. 5), Proc. Highway Research Board, 36, (1957), Reprint No. 105 (57-1)

K. E. Knudsen

W. J. Eney

Prestressed Concrete Bridge Members
Progress Report 5

ENDURANCE OF A FULL-SCALE PRE-TENSIONED CONCRETE BEAM

by

K. E. Knudsen and W. J. Eney

(Not for Publication)

This work has been carried out as a part of
an investigation sponsored by the following:

Americal Steel & Wire Division of U. S. Steel
Concrete Products Company of America
Lehigh University
Pennsylvania State Highway Department
Reinforced Concrete Research Council
Research Corporation
John A. Roebling's Sons Corporation
U. S. Bureau of Public Roads

Fritz Engineering Laboratory
Department of Civil Engineering and Mechanics
Lehigh University
Bethlehem, Pennsylvania

1 April 1953
Fritz Laboratory Report 223.5

CONTENTS

ABSTRACT

Prestressed concrete beams are being put to use in buildings and highway bridges in increasing number and span lengths. By experiments and experience adequate safety is proved for such beams under static loading; the same is not, however, the case for repeated service loads. Only relatively few tests in the U.S. and abroad support the designer's faith in satisfactory lifetime performance, and no prestressed beam in this country is yet nearly old enough to verify this requirement.

In line with the traditional desire of responsible engineering of proving structural adequacy by tests the Lehigh investigation of prestressed concrete bridge members was undertaken. The prime objective of this investigation is to observe the behavior of actual full-size members when subjected to the maximum magnitide and number of loads and overloads to be expected during the lifetime of a corresponding structure. The results of the first of such tests, on a strand-reinforced pretensioned highway beam, are reported in this paper.

The beam suffered no damage during 1,300,000 repetitions of equivalent H20-S16 truck loading for which it was designed and subsequent 100,000 repetitions of 54% overload. This treatment simulates at least 100 years of service under present highway traffic load magnitudes and density. When finally tested to destruction the beam failed by crushing of the concrete at a load corresponding to dead load plus 4.2 times design live load including 30% impact, or 3.1 times the dead load, live load and impact. No bond or steel failure occurred.

A. INTRODUCTION

1. Objectives

During the last few years prestressed concrete has gained wide use in the United States. The rapid utilization of this new material has been possible partially because of the favorable experiences in Europe during the past two decades.

Numerous tests have been performed or started in this country to verify the validity under American conditions of results obtained elsewhere and to seek information that has not so far been available. Of the latter group of research the investigation of the behavior of prestressed concrete members under repeated loading is perhaps the most important since one of the main applications of prestressed concrete has been in highway bridges.

Some tests of the effect of repeated loading have been performed in Europe. Differences in material properties, construction practices, and magnitude and frequency of highway loadings makes the direct use of such data as are available unsatisfactory. Moreover, factors such as geometric similarity and mass effects cause serious difficulties in interpreting test data in case small-size models are used.

The present investigation was therefore initiated in 1951 with the ultimate purpose to furnish data that may aid in the preparation of design specifications. Specifically, the objectives are:

1) Comparison of beam behavior under static loads with that predicted by available methods of analysis.
2) Observation of the effect of a simulated lifetime service through the application in the laboratory of an equivalent number of maximum design loads and overloads.
3) Comparison of the structural adequacy of prestressed beams of various systems, each representing a typical economical design for the span length (36 ft.) and the loading (AASHO H20-S16-44 truck loading) in question.
4) Comparison of the isolated beam behavior with the behavior in composite bridge decks.

2. Test Program

The above objectives are pursued through the following general test program:

1) Pilot beam tests.
2) Full-scale beam tests.
   a) Pretensioned 38-ft. beam.
   b) One-unit non-grouted post-tensioned 38-ft. beam.
   c) Possible additional full-scale beam tests.
3) Tests of short-span bridge of several pretensioned beams to determine composite bridges behavior.
4) Test of an actual structure.
5) Study of bonding characteristics of prestressing strands.

Phase (1) above consisted of five 8" x 12" x 12' - 0" beams, giving a comparison of various prestressing systems and regular reinforced concrete in model beams subjected to static third-point loading, as reported upon earlier.[1,2,3]* The experimental techniques were also studied and improved during the pilot investigation.[4] Step (2a) in the above program is reported upon herein.

Phase (2) in this investigation involves a very ambitious testing program, carrying full-scale beams through a full lifetime service. The number of individual tests must therefore necessarily be kept small. A complete separation of variables affecting the beam behavior is not economically feasible, and the objective of phase (2) of the investigation is limited to a comparison of the overall behavior of various types of prestressed beams as represented by typical designs according to the best current American practice for each type.

*Numbers refer to List of References.

The handling and transport of 38-ft. prefabricated, pretensioned beams presents no difficulties; yet this length is large enough for post-tensioned members to be competitive under present conditions. The test set-up is greatly simplified by maintaining a constant length for the different types of test beams. Thus the length 38 ft. with a simple span of 36 ft. between supports was selected.

As appears from Objective (2) above, it is not a purpose of this investigation to establish fatigue load limits for the members tested. Fatigue type failures are not specifically sought, and are of interest only to the extent such failures would limit the comparatively small capacity for load repetitions required during a normal lifetime service. The tests are therefore referred to as "repeated load tests" and the term fatigue is avoided as misleading.

3. First Full-scale Test Beam

a) Description:

As the first full-scale test beam was selected a precast, pretensioned, hollow-core rectangular type beam commercially available in Pennsylvania, Indiana, Wisconsin and Illinois. During the last few years about 75 bridges of 18-ft. to 50-ft. spans have been constructed with these beams for the Pennsylvania State Highway Department. The 38-ft. test beam is shown in Figure 1.

The beam is rectangular, 36" x 21" in cross-section, except for keyways provided near the top of the sides. The beams are placed side by side to form the bridge deck, tied together with steel rods and the keyways dry packed or grouted. To save weight two hollow longitudinal cores 12-1/2" Ø are provided except at the points of lateral tie rods and at the ends. The test beam is prestressed by 40 strands of 5/16" diameter. Four plain reinforcing rods are provided on the top supporting wire mesh across the top and sides of the beam.

b) Manufacture:

The beams are manufactured, several at a time, on 120-ft. long casting beds. After placing and stressing the strands (Figs. 2 & 3) the side wire mesh and the side forms are provided and the pouring operation started (Fig. 4). The bottom layer of concrete covering the strands consists of a mortar-rich mix in order to ensure good bond with the strands. The hollow cores are provided by placing stiff cardboard tubes on this bottom layer (Fig. 5). The pouring continues with a stiffer mix after placing of the top wire mesh.

The concrete is covered with vacuum mats as soon as the forms are filled, and the concrete is vacuum-treated through the side forms and top mats for about one hour (Fig. 6). The forms are stripped shortly thereafter. The regular manufacture procedure calls for curing with wet burlap immediately after stripping until transfer of prestress. The test beam could not be moist cured, however, since the SR-4 electric resistance strain gages were applied to the concrete surfaces the day after pouring in order to yield information during the transfer of prestress (Fig. 7). The prestress was transferred to the concrete four days after casting by burning off the strands, starting at the far end of the bed about 80 ft. from the test beam. On the following day the beam was lifted from the bed onto a truck for the 40 miles transport to Fritz Engineering Laboratory.

A more detailed description of the manufacturing process for this type of beam may be found in Ref. 5.

B. TESTING PROCEDURE

1. Simulated Service Loading

The objective of the repeated load tests on full-size prestressed concrete beams is to observe the effect of the maximum magnitude and the maximum number of loads and overloads that a corresponding bridge member may be expected to experience during an estimated lifetime.

The 1949 AASHO "Specification for Highway Bridges" and recent traffic volume surveys are aids in determining these loadings; however, considerable judgment is obviously needed in the process of arriving at reasonable equivalent experimental loadings.

a) Magnitude of Design Live Load:

The basis for the design live load on the test beam is the AASHO H20-S16-44 loading (Spec. 3.2.5.c) with the minimum rear axle spacing of 14 ft. (Fig. 8a). This is the most severe AASHO specification loading which exceeds the legal limits in all of the United States. Quoting from a 20 March 1953 letter from Mr. E. L. Erickson, Chief, Bridge Branch, U. S. Bureau of Public Roads:

> "The permissible types, sizes and weights of trucks operating on the highways are governed by the laws of the individual States. Most States permit loads of 18,000 pounds on any single axle and 16,000 pounds on each of two axles spaced at least 4.0 feet apart. A few States permit single axle loads slightly greater than 18,000 pounds. The H20-S16 truck, with its 32,000-lb. single axles, is not a legal vehicle in any State. It should be regarded only as a standard group of axles, which, when applied to a structure, produces stresses approximately equal to the composite effect of the various vehicles in the traffic. This explains why relatively few single axles weighing more than 18,000 pounds and relatively few dual axles with a combined weight exceeding 32,000 pounds are recorded in traffic surveys. We believe, however, that many of the trucks weighed and listed produce moments in a 36-ft. span approaching those of the H20-S16 truck."

To the static H20-S16-44 loading is added the effect of impact according to AASHO 1949 Spec. 3.2.12.c,

$$I = \frac{50}{L + 125} \leq 0.30$$

where the span length in question, L = 36 ft., yields I = 0.31. Thus, 30% is added for impact to the loads shown in Fig. 8(a).

The fraction of a wheel load to be carried by each longitudinal beam is determined by AASHO 1949 Spec. 3.3.1.b. Since only a 2-in. concrete or bituminous topping is normally used on this type of beam the most severe case of S/3.75 is used. With beam spacing S = 3 ft., equal to the width of the members, the fraction of a wheel load to be carried by each beam is 3/3.75 = 0.80.

The resulting actual beam load and moment diagram for the critical truck position are shown in Fig. 8(b) and (c), together with the experimentally used third-point loading producing the identical maximum moment. The weight of the topping, 30 lbs. per sq. ft., is also included in the third-point loading.

b) Number of Design Live Loads:

The total number of maximum design live loads to be expected during the lifetime of the structure is the product of the load frequency and estimated lifetime, both of which are subject to judgment.

Ref. 6, p. 6, lists distribution of wheel loads on commercial vehicles on typical roads in seven mid-western states as obtained from 1948 state planning surveys. The H20-S16 wheel load falls in the heaviest group listed (more than 15,000 lbs. static wheel load), which is represented only under highways Class I, "Primary Route in or Near a Metropolitan Area," with a maximum frequency of 10.1 wheel loads per day in both directions. The equivalent number of H20-S16 trucks in each direction is 2.5 per day. Ref. 7 points to an average increase in traffic volumes of 9% per year. Projecting 25 years ahead from 1953, the maximum number of H20-S16 trucks in each direction should average about 10 per day over the

next 50 years. Although the number of overloaded trucks per 1000 weighed has recently showed a decline[7] this figure may be raised to 20 per day due to the great uncertainties in predicting traffic developments over such a long period.

It may prove even more difficult to arrive at an estimation of the expected lifetime of highway bridges of about 36-ft. span length. Assuming 50 years and the frequency arrived at above the total number of maximum design loads is 365,000.

The test beam has been subjected to 1,300,000 repetitions of equivalent H20-S16-44 loading which is sufficiently in excess of the estimated 365,000 repetitions to cover any uncertainties as to the adequacy of the experimental loading.

c) Overloads:

The experimental treatment of the test beam should also reflect the well-known fact that our highway bridges are frequently subjected to significant overloading. The average weight of loaded trucks and truck combinations on U.S. highways in 1951 was 42,500 lbs.[7] which is well below the 72,000 lbs. of an H20-S16-44 truck. However, the following table[7] of number of truck and truck combinations, per 1000 loaded and empty vehicles, that exceeded any of the permissible load limits recommended by the AASHO shows the overload frequency and magnitude to be expected.

From Ref. (7)	No. of trucks per 1000 loaded and empty vehicles that were overloaded by more than					
	0%	5%	10%	20%	30%	50%
Summer 51	72	52	35	16	7	1
Summer 50	92	68	46	21	10	3

It appears that few or no loads may be expected to exceed 150% of the permissible limits.

In addition to the 1,300,000 repetitions of design live load the test beam was subjected to 100,000 cycles of 54% overload. This corresponds to 72 overloaded trucks per 1000 loaded vehicles, which is considerably in excess of the above traffic survey volume both with regard to frequency and to magnitude.

On the background of the above discussion the experimental treatment given the test beam may safely be assumed to be more severe than the actual lifetime service at any highway bridge location.

2. Repetitive Loading Machine

Figure 9 gives a general view of the repetitive loading machine which was designed and constructed in Fritz Engineering Laboratory for the purpose of these tests. The machine is capable of applying equal third-point cyclic loads of up to 25,000 lbs. to beams up to 36 ft. span at variable frequency from 1/8 to 250 cycles per minute.

A detailed description of the machine will be given in a separate paper and only a brief outline is included here.

A 50HP motor (Fig. 10, a) operating a variable-volume pump (Fig. 10,b) supplies the pressure to two 15,000 psi hydraulic tension jacks under the beam third-points. A solenoid-operated four-way valve (Fig. 10, c) is inserted between the pump and the jacks. The solenoid is activated by a photoswitch timer which allows the independent selection of the loading and unloading periods between 0.1 sec. and 4 minutes.

By regulating the pressure of the oil supplied to the jacks, the periods of loading and unloading, and the volume of the pump, the moment-time diagram for the centerline section of the beam may be adjusted to equal closely that due to the passing of an H20-S16-44 loading at various speeds. The speed selected for these tests is 40 mph giving a load frequency of one cycle per second. The corresponding moment-time diagrams for the actual and the experimental loading are shown in Fig. 11a.

During the testing the applied force at the beam third-point was registered by the one channel of a two-channel automatic strain recorder. This recorder amplifies the combined output of four SR-4 dynamic electric resistance strain gages mounted longitudinally and circumferentially on the jack tension rod and makes a continuous trace of this force on a calibrated oscillograph paper strip (Fig. 11b).

The other channel simultaneously registered the strain as measured by any one of the SR-4 strain gages which were placed on the concrete surfaces or on the steel strands within the beam.

The repetitive loading machine capacity is not large enough to apply the 54% overload directly. For this part of the test, therefore, the beam was subjected to an initial dead weight loading of 6400 lbs at each third-point as shown in Fig. 12. This loading corresponds to 36% of design live load, the testing machine producing cycles from 36% to 154% of design live load.

The static test loads were determined by means of the hydraulic pressure gage which was calibrated against SR-4 strain gage readings on the calibrated jack rods. After the fifth static test a recalibration showed that a drift had developed in the pressure gage readings causing increasing loads to be applied during the static tests Nos. 2-5. Readings from these tests are corrected for the error which for the sixth static test amounted to 15% overload. During the repeated load tests the correct load, as determined by means of the jack rod SR-4 gages, was applied throughout.

The test frame itself (Fig. 9) consists mainly of two 36WF beams, with the necessary bracings and stiffeners, whereupon the test beam rests on end pedestals 36 ft. apart. One test beam support is hinged; the other end of the beam rests on a rocker.

3. Instrumentation

a) Slip of Strands:

In order to detect any bond failure causing slip of the strands the protruding ends of the strands were covered by metal caps and their distance from a slip rig, securely fastened to the concrete beam (Fig. 9), was observed by means of a 1/1000 inch dial gage. Both ends of all 40 strands were observed in this manner.

b) Deflections:

The beam deflections at the centerline and quarter-points were measured by means of mirror scales attached to the beam at these points as shown on Fig. 13. The readings were referred to the beam centerline at the supports by means of a taught wire.

In certain tests also a 1/1000 in. deflection dial under the beam center-point was used. During the latter part of the destruction test readings were taken on the scale mirrors by means of a level instrument placed at a safe distance.

Deflections were observed only during the separate static load tests, and no continuous zero reading was carried through the complete test sequence. However, visual inspection revealed a permanent deflection of about 3/8 in. due to the 1,400,000 load and overload repetitions since the initial camber of this magnitude was just lost.

c) Strains:

Strains at the concrete surface were measured partly with 10 in. Whittemore gages and partly with SR-4 electric resistance strain gages of types AR-1 (rosettes, 1 in. gage lengths) and A-9 (single 6 in. gage length) as indicated in Figs. 13 and 14. The concrete surface at each SR-4 gage location was dried with heat lamps after stripping. Steel points for 10 in. Whittemore gage readings were successfully glued to the concrete by Duco cement, as were the SR-4 gages (Fig. 15). The difficulty in maintaining a reliable zero SR-4 gage reading over a longer period of days made the use of Whittemore gage readings desirable. The SR-4 gage, however, has the advantage of allowing automatic strain recording during the cyclic loading.

Strains in the steel strands were observed by means of water-proofed SR-4 gages applied along single wires of the strands at interior locations shown in Fig. 14. This experimental technique which involves swaging of the 7-wire strand to a nearly-cylindrical shape over a 4-in. length is described earlier.[4] Recent tests by the John A. Roebling's Sons Corporation, however, indicates that the swaging operation adversely affects the creep characteristics of the strand. Care must therefore be taken in interpreting the strain readings, at least at higher stress levels.

d) Cracks:

The detection of cracks on the concrete surface was facilitated by the application of white-wash (Fig. 9). The cracks were mapped at various stages. No attempt was made to report the crack widths.

4. Testing Sequence

The detail test program for the beam is outlined below and shown in Fig. 16:

Age of Beam (days after casting)	Load Magnitude (% of design live load)	Static Test (event)
-1	---	During pretensioning
0	---	After casting, Aug. 23, 1952
4	0	Before and After Release
4	0	After Transport to Lab.
35	0-100	Before Cyclic Loading
37-50	0-100	(300,000 cycles)
58	0-100	After 300,000 Cycles
62-78	0-100	(300,000 cycles)
79	0-100	After 600,000 Cycles
80-88	0-100	(400,000 cycles)
88	0-100	After 1,000,000 Cycles
114	0-100	Before Continuing Cyclid Loading
114-119	0-100	(300,000 cycles)
130	0-100	After 1,300,000 Cycles
135	0-155	Before Overload Cycles
136-139	36-155	(100,000 overload cycles)
156	0-175	After Overload Cycles
166	0-350	Destruction Test Attempt
167	0-370	Destruction Test Attempt
169	0-410	Destruction Test; Center Loading

C. MATERIAL PROPERTIES

1. Concrete

a) Mix:

Air-entraining portland cement (Type IA) was used in the beam. A natural sand and a crushed gravel of gradings as shown in Fig. 17 were used in the weight ratio 39% sand and 61% gravel resulting in a total aggregate fineness modulus of 4.49. The total aggregate grading is shown in Fig. 17 in comparison with the recommended Fuller and EMPA curves. No admixtures were used in the concrete.

Two concrete mixes were used in the beam. The strands were covered with a mix containing slightly more water than the mix used in the rest of the beam as shown in Table 1. The close spacing of the strands both horizontally and vertically made desirable a more plastic mix than was required above the strands. The w/c-ratio for the major upper part of the beam was 0.35, the measured air content 4.2%, and the slump 4.5 in. The concrete was mixed for 2 minutes.

The beam was vacuum-treated after pouring and thus the effective water-content reduced at least for a portion of the beams cross-section. In order to obtain an approximate indication of the actual mix proportions the water drained from three vacuum-treated 6" x 12" test cylinders was measured. The unit weight after vacuuming was also determined. The resulting mix proportions are shown in Table 1, indicating an increase in c/w-ratio of 10% with an expected increase in compressive strength of the same order. It should be remembered that these test results from vacuum-treated cylinders are only indicative of the corresponding effect on the actual beam concrete.

b) Concrete Cylinder Tests:

Standard 6" x 12" test cylinders were poured and vacuum-treated simultaneously with the test beam to yield information on the compressive strength f'_c and modulus of elasticity E_c at various ages. The f'_c-cylinders were air-stored in the laboratory for 33 days, and from then on kept in a moistroom. The E_c-cylinders were air-stored throughout with one exception.

The individual values obtained for E_c and f'_c are shown in Table 2 together with their averages. As expected from the mix data (Table 1) the concrete covering the strands to about 5 in. from the bottom is of somewhat poorer quality. In order to obtain good bond and a high cracking load this concrete should be as good as that in the rest of the beam. A more workable mix desired for embedding the strands thus be obtained by reducing the aggregate content and not by increasing the amount of water.

c) Correlation with Beam Concrete:

Curing conditions for test cylinders can never be made identical to those of the actual concrete they represent. Some interpretation of cylinder test data will therefore always be required except for standard acceptance tests. Considering the relative curing conditions for the beam (air cured, larger volume) and for the cylinders (unintentionally air-cured for 33 days, moist cured thereafter), the following values are assumed to be closely representative for the concrete in the test beam:

AGE (days)	EVENT	E_c (ksi)	f'_c (psi)
4	Release	3330	3300
35	1. Static Test	3500	5000
58	2. Static Test	3600	5500
79	3. Static Test	3700	5600
88	4. Static Test	3750	5700
114	5. Static Test	3800	----
130	6. Static Test	3920	----
135	7. Static Test	3930	----
156	8. Static Test	3950	----
169	Destruction Test	4000	6000

D. PREDICTED* AND OBSERVED BEAM BEHAVIOR

1. Deflections

The first application of design live load caused a centerline deflection of 0.54 in. which very nearly equals the predicted value 0.55 in. (p. 79). The subsequent increase of the concrete modulus of elasticity with time (p. 15) will tend to reduce the deflections. On the other hand, the repeated loading above the cracking load must be expected to cause progressive cracking resulting in increasing deflections. These opposing effects resulted in small variations in deflections with a small increasing tendency as the repeated loading progressed:

STATIC TEST No.	$\delta_{L/2}$		$\delta_{L/4}$	
	in.	%	in.	%
1	0.54	98	0.38	97
2	0.52	96	0.37	97
3	0.59	111	0.43	116
4	0.58	111	0.40	108
5	0.55	107	0.38	104
6	0.53	104	0.37	103
7	0.47	93	0.33	93
8	0.71	144	0.46	132

In the above table the observed centerline and quarter-point deflections are given in inches and in percent of the predicted value (p. 79) with regard to the increasing modulus of elasticity. The same data are pictured in Fig. 19.

The effect of 100,000 loadings to 154% of design live load appears from a comparison of static test Nos. 7 and 8 (Fig. 19). The design live load centerline deflection increased from 93% to 144% of the value predicted with no regard to cracking, which in view of the severe loading is an expected change.

The increase with load of the centerline and quarter-point deflections is shown in Fig. 20. Experimental points from various static tests are plotted in comparison with the theoretical load-deflection curve using the modulus of elasticity at the beginning and at the end of the 4 1/2 month testing period. The experimental curve for the first static overload test (No. 7) and that of the static test following the 100,000 overload repetitions (No. 8) are also shown. For larger overloads the repetitions caused an appreciable deflection increase; for working load the increase was 50%.

Cracking rapidly reduces the moment of inertia of the section and thus shows up as a change in the slope of the load-deflection diagram. Such a change is noticeable for the 8. static test at about 12.5 kip third-point load (Figs. 20, 21) which agrees with the predicted crack opening load at that age (See Table, p. 76).

Destruction of the beam was first attempted with third-point loading but was not successful due to insufficient jack capacity. However, valuable information resulted from this attempt as shown in Fig. 21. The beam was first loaded to 86% of the moment later causing failure in a concentrated center load test. This loading caused a centerline deflection of 8.7 in. of which only 1.3 in. remained after removal of the load. Overnight the beam recovered slightly to 1.1 in. permanent deflection. A second loading up to 97% of the predicted ultimate live load moment, or 91% of the actual maximum moment, gave 9.7 in. centerline deflection, of which 2.2 in. remained after unloading. The predicted ultimate load and the predicted ultimate deflection (9.4 in., p. 80) is represented by a point on Fig. 21, falling close to the experimental curve.

It is noteworthy that the beam, after having sustained 86% and 91% of its ultimate load, showed only a modest permanent deflection and closing of nearly all cracks.

*See Appendix, "Stress Analysis of Pretensioned 38 ft. Test Beam."

The assumed concrete stress-strain diagram is given in Fig. 46.

2. Steel Strands

The 40 5/16" ø strands used in the test beam consist of six 0.100 in. diameter cold-drawn wires wound around a 0.109 in. diameter center wire. The strand is of a time-temperature treated type made for pretensioned concrete construction; the minimum guaranteed ultimate strength is 260,000 psi and the recommended design stress 150,000 psi.

The swaging operation required for application of SR-4 strain gages on the strand[4] is a cold-working process which must be expected to alter the elastic properties. The modulus of elasticity to be used in interpreting the SR-4 readings was therefore determined by an SR-4 gage on a swaged strand coupon test. The pretensioning force at the casting bed was checked by means of the strand elongation (see p. 71), and for this purpose Young's Modulus of the un-swaged strand was determined by a mechanical extensometer over a 20-in. gage length.

The results of both these tests are shown in Fig. 18. The modulus of elasticity is 27,700,000 psi for the un-swaged strand and 27,300,000 psi for the swaged portions. The ultimate strength is 275,000 psi. The manufacturer's value for the 0.2% permanent set proof stress is 240,000 psi and for the ultimate elongation is in excess of 4% over a 24-in. gage length.

The deflected shape of the beam at various stages during the third-point load destruction tests are shown in Fig. 22. As the center portion of the beam is progressively cracking the curvature increases more rapidly there than towards the supports. This behavior was quite pronounced in the final center-load destruction test towards the end of which a "hinge" developed at the center (Fig. 23). This hinge remained after unloading the fractured beam (Fig. 30) which otherwise returned to its previous straight shape.

The load-deflection curve for the final destruction test using a concentrated center load is shown in Fig. 24. Failure took place at an imposed load 9% larger than predicted. The ultimate deflection was 11.5 in.

The destruction test results are summarized in Table 3.

2. Slip

In order to detect any appreciable slip during the release of the strands from the pouring bed marks were put on each strand end about one inch from the end concrete face of the beam. The distances of these marks to the concrete face did not show any change that could be measured by a rule (Accuracy about 0.03 in.).

The results of the more accurate slip measurements (p. 11) throughout the testing period are shown in Fig. 25. Since the movements were not affected by the loading on the beam only one reading from each static test is shown. The accuracy of the readings is estimated to $\pm 4/1000$ in. This is supported by the observation of movements of this order out from the beam end face, which is actually inconceivable. Applying this criterion in interpreting Fig. 25 it is seen that only a few strand ends exhibit a tendency of progressive movement of a magnitude that can be ascribed to actual slip. West strand end No. 4 clearly indicates some slip and a few others (West end Nos. 5, 6, 34 and 40) show slip tendency. The magnitudes, however, are small. Thus the observed 0.033 in. slip of west strand end No. 4 would result if the end bond anchorage of this strand shifted 9 in. into the beam. As a uniform relaxation throughout the beam length the 0.041 in. total slip of both ends of this strand corresponds to a stress loss of 2600 psi. This strand like the others did not show appreciable further slip due to the overload cycles or the destruction loading.

The average movements during the test program of all 40 strands at each end of the beam give an overall measure of the slip tendency. As basis for these averages is taken the maximum amplitude for each strand end movement as pictured in Fig. 25. The averages, which thus include the effect of reading inaccuracies, are:

East end, ave. movement	0.00385 in.
West end, ave. movement	0.00425 in.
Total average movement	0.00805 in.

Again these movements may be interpreted as a shift of end bond anchorage into the beam of 1.1 in. and 1.2 in. for the east and west ends, respectively, or as a total relaxation of prestress throughout the beam of 520 psi. The first interpretation is considered to be the actual cause of the observed movement, in agreement with bond studies* which show that the end bond anchorage length increases with time. The corresponding end movement of the strands is not to be regarded as slip insofar as this term is associated with bond failure.

Thus, no slip indicating end bond failure was observed at any stage of the repeated loading and destruction test of the beam.

3. Cracks

The cracks that occurred at the various stages during the test program are mapped in Fig. 26 for the east half of the beam and in Fig. 27 for the west half. These are the cracks that were visible to the naked eye although a magnifying glass was used in determining the extent of the cracks.

Cracks occurred on the top surface near the ends at release of prestress, and these cracks extended around the lifting hooks during the handling as shown by heavy lines in Figs. 26 and 27. The design stress due to prestress at these locations is 354 psi tension. The lack of moist curing, the exposure to

*Eidg. Materialprüfungs - und Versuchsanstalt, Bericht No. 162, DIE MATERIALTECHNISCHE GRUNDLAGEN UND PROBLEME DES EISENBETONG, Zürich, 1950, p. 231, "Vorgespannter Beton."

drying from sun and wind, and the effect of handling and truck transportation are factors responsible for this cracking.

During the first static test cracks developed between load points on the bottom face at an average spacing of roughly 8 in., the cracks extending an average of 4.5 in. upwards on the beam sides (Figs. 26 & 27). The predicted crack opening load at this time was 14,200 lbs. or 81% of design live load (p. 79). The neutral axis according to the predicted stresses (p. 74) was 3.0 in. from the bottom. Since the beam surfaces were more subjected to drying and shrinkage than the interior the cracks must be expected to extend further up along the side surfaces than inside the beam. As the number of load repetitions increased so did the extent of cracking until after 1,300,000 cycles the average crack length from the bottom reached 9.5 in. The predicted location of the neutral axis was then 3.8 in., and the crack opening 74% of the applied design live load.

During this loading cracks also developed at the top edges which presumably were under compressive bending stresses. This supports the above assumption of residual surface tension due to non-uniform shrinkage. Fine longitudinal shrinkage cracks also occurred along the sides at the junction of the wetter concrete covering the strands and the dryer mix above. Similar longitudinal shrinkage cracks along the keyways are believed caused by mortaring the keyway corners after removal of the side forms, or possibly by time lag and mix differences between individual lifts during pouring. Longitudinal cracks along the bottom surface (Figs. 26 and 27), at about the beam width center and quarter-points, are believed initiated by shrinkage but later during the destruction test opened in parts to 0.5 in. width (Fig. 29).

The overload cycles further extended the crack pattern as shown by double lines in Figs. 26 and 27, which reach an average of 16 in. from the bottom edges. Also these cracks, however, closed completely upon removal of the live load.

The crack pattern due to the third-point destruction load attempts was an extension of the pattern shown in Figs. 26 and 27, and the cracks very nearly closed after removal of the load that reached 91% of the ultimate. The appearance of the center region after failure produced by center loading is seen in Fig. 28 showing the sides of the beam and in Fig. 29 for the bottom surface. The diagonal cracks near mid-height of the beam (Fig. 28) became pronounced at about 93% of the ultimate load. In these pictures the fractured beam is still carrying $M_D + 2.0\ M_L$ with a deflection of 13.7 in.

From the above discussion it is seen that due to the low prestress being applied the beam cracked below working load as was expected (predicted cracking load 81 to 73% of design live Load). During the repeated loading the cracking grew more extensive than predicted on the basis of static loading but all structural cracks closed upon removal of the live load, also after the overload repetitions. The repeated loading beyond cracking put the beam to a test far more severe than had the beam been fully prestressed.

4. Concrete Bending Stresses

a) Release of Prestress:

At release of the strands from the bed the combined prestress and counter-acting dead weight caused concrete fiber strains which were measured by SR-4 and Whittemore gages. These strains were translated into stress using the proper concrete modulus of elasticity (p. 15) and are shown in Fig. 31 in comparison with the predicted values.

The strain readings were influenced by unfavorable outdoor conditions with large temperature increase and differential about sunrise. Also, the very green concrete was most likely affecting the moisture-sensitive electric strain gages. Nevertheless, a general verification of the predicted trend of stresses was obtained as shown in Fig. 31. The top fiber at the supports is subjected to tensile stress of a magnitude (350 psi) that in combination with shrinkage and handling were large enough to cause cracking (Figs. 26 and 27). Near mid-span the prestress + dead weight caused a small compressive stress (70 psi) which was not sufficient to prevent shrinkage cracks at the edges (Figs. 26 and 27). The bottom fiber compressive stress is reduced by the dead weight from a predicted 1320 psi at support to 920 psi at mid-span.

b) Working Load:

Under the better controlled laboratory conditions satisfactory agreement was obtained between predicted and observed concrete stresses due to live load. A comparison is offered in Fig. 32 for the static test preceeding any repeated loading. For the top fiber, which is in compression, excellent agreement was obtained with the 10 in. Whittemore strain gage readings, while the 1 in. and 6 in. SR-4 gages

indicate lower stresses. At design live load the center region of the bottom fiber is cracked and less good agreement must be expected between readings over different gage lengths and with the predicted values. In a strict sense, strains measured over a cracked surface cannot be directly translated into stresses. Figure 32 shows, however, that also the overall bottom fiber behavior is predicted with sufficient accuracy by assuming a homogeneous section (p. 73) although the crack-opening load is exceeded by 25% (p. 76).

The average top fiber stress at mid-span due to the first applications of design live load (Table 4) was 90 to 99% of the predicted stress. The 1,300,000 repetitions of this load produced a modest increase in top fiber stress consistent with the upward shift of the neutral axis which followed the progressive cracking. A maximum stress equal to 119% of the predicted was observed. The inconsistencies in stress changes with increasing number of load repetitions (Table 4) is believed to reflect experimental inaccuracies.

The corresponding effect on the bottom fiber is given in Table 4 in terms of strain rather than stress. These strains picture the increase in amount of cracking which prevents the concrete from carrying a corresponding increase in stress. Before cyclic loading the design live load strains were 95-97% of the predicted, an agreement which parallels that for the top fiber indicating little influence of the cracks at this stage. Consistent with the crack pattern change (Figs. 26, 27) repeated loading caused an appreciable average bottom fiber elongation, reaching a maximum 139% of the predicted value after 1,300,000 design load cycles.

The 100,000 repetitions of 54% overload, as seen from the final failure test, were not destructive but left definite signs of distress. The effect on deflections (p. 17) and cracking (p. 22) is mentioned earlier. The top fiber stress at midspan increased to 109 - 134% of the predicted (Table 4), and average bottom fiber strains as high as 232% of those in a homogeneous section show appreciable crack widths.

The above discussion is limited to the separate stresses and strains due to each individual live loading and does not include permanent effects of the repeated loading or of time. This effect will be discussed later in connection with losses in steel prestress.

c) Cracking Load:

The initial third-point cracking load, counting upon the resisting contribution of the concrete modulus of rupture, is calculated to be 25.8 kips or 1.45 times design live load at the time of the first static test (p. 76). Theoretically this load may be reached once, and forever after the cracks thus caused will open up at a load giving zero bottom fiber stress. This latter load is referred to as the crack-opening load.

As discussed earlier (p. 21) non-uniform shrinkage must be expected to cause residual surface tension. Under good curing conditions this residual stress may not be sufficient to initiate surface cracks even after long time exposure in the open. It will, however, materially reduce the theoretical cracking load in which laboratory test results obtained on carefully cured specimens tend to give unwarranted confidence. Discounting any tensile strength of the concrete, the above cracking load of the test beam is reduced to 14.2 kips or 0.81 of the design live load (p. 76) at about which load cracks were actually observed during the first loading.

The highly stressed special steel used in prestressed concrete construction is believed to be appreciably more sensitive to corrosion than regular reinforcing bars. Certainly over salt water and where full design impact will be realized crack-free design should be given serious consideration. Although the present test showed that cracks were not structurally detrimental to a long life's hard service consideration of corrosion resistance may warrant the specification of crack-free design. If so, the more rigid criterion

$$\text{Crack-Opening Load} \geq 1.0\ (M_D + M_L)$$

is recommended in place of the commonly used

$$\text{Cracking Load} \geq 1.5\ (M_D + M_L).$$

A 35% higher prestressing force would have achieved this effect on the test beam, and could be obtained by using the full allowable initial prestress f_{si} = 165,000 psi (p. 80) and by adding 2% to the steel area. The corresponding increase in danger of cracking from the top near supports would not affect the strands. The top is also protected by the surfacing.

In Fig. 33 the predicted crack-opening load (p. 76) is compared with experimental values as furnished by marked changes in rate of increase in deflection (Fig. 20), concrete and steel strain (Fig. 39), and by

visual inspection during the loading. Although these means furnish only approximate values a fair agreement with predictions is apparent. The theoretical cracking load was never reached as the very first loading caused visible cracking between 14 and 17 kip third-point loading (in Fig. 33 plotted as 15 kips). Moist curing of the beam would probably have raised this value.

d) Ultimate Load:

The development of compressive concrete strain in the top fiber at the centerline section during the third-point destruction load test is shown in Fig. 34. These values were obtained from the strain distribution across the depth of the beam as determined from SR-4 strain gage readings.

The shape of this diagram is very similar to the load-deflection diagram, Fig. 21. The concrete strain closely follows the predicted up to the crack-opening load. Failure was not obtained in this test which was interrupted at a maximum compressive strain of 2230 micro-in/in., corresponding to 5600 psi compressive stress (Fig. 46). Failure was predicted at 3000 micro-in/in. strain or 6000 psi stress. The shpae of the curves, Fig. 34, indicate that this prediction is reasonable.

Figure 34, as does the load-deflection diagram Fig. 21, shows that the permanent set caused by loading to within nine tenths of the fracture moment was modest and not detrimental to the final carrying capacity.

The strain measurements across the beam depth at center also made it possible to follow the shift of the neutral axis. Using the foregoing, and the predicted values (p. 74) for the smaller effect of prestress + dead weight, the resulting upward shift of the neutral axis with increasing moment is shown inserted on Fig. 34. At 62.0 kip the observed location of the neutral axis was 4.02 in. from the top fiber. The predicted location at failure, 63.7 kips, is 4.07 in. from the top (p. 78). This agreement must be ascribed to the method used for ultimate load prediction which satisfies both the equilibrium conditions and the compatibility condition that originally plane sections remain plane during loading. In contrast, the approximation used to compute the steel stress after cracking (p. 76) does not give linear strain distribution across the section. Although the resulting predicted steel stresses are close to the actual (Figs. 38, 39, 40) the corresponding predicted location of the neutral axis ("Crack Length," p. 77) becomes increasingly too low as the load increases beyond crack-opening load.

5. Steel Stresses

a) Losses in Prestress:

The evaluation of losses in prestress to be assumed in design entails some uncertainty and an experimental verification was therefore sought in this test. Whittemore gage points were placed along the upper (2 in. from top) and lower fibers (at average strand level) before release of prestress. Readings from these points yielded information on the elastic shortening due to prestressing and on the subsequent combined creep and shrinkage of the concrete. The results are compared with the predicted values (see "Stress Analysis," p. 71) in Fig. 35 for several locations along the beam and for various stages of the test. The average shortening along the beam length from Fig. 35 is given in Fig. 36 as a function of time in comparison with the assumed rate of loss (Fig. 43).

The elastic loss at release is computed to be 8300 psi (p. 74) or 300 micro-in/in. fiber shortening. Readings taken shortly after release will contain some creep which starts out at its fastest rate of increase. The agreement between predicted and observed elastic fiber shortening in Fig. 35 is therefore quite satisfactory. The average observed shortening along the beam was 340 micro-in/in. as shown in Fig. 36.

Fiber shortening due to creep and due to shrinkage cannot be directly separated experimentally by observations on the test beam. Their combined progressive effect is illustrated in Fig. 35. The final observation (8. Static Test) agrees perfectly with the prediction along the middle third of the span except at the solid center diaphragm. However, the extensive cracking over this length is believed to have caused some permanent elongation counteracting the creep and shrinkage shortening, this in spite of the cracks being visually closed in the unloaded state when the readings were taken. The higher experimental values towards the support is therefore probably more representative for an uncracked section. In fully prestressed or nearly crack-free design the assumed ultimate shrinkage strain loss of 0.0003 in/in. may therefore be inadequate. Remembering that the test beam was not moist cured this value is most likely too low. The assumption of a total shrinkage of 0.0006 in/in. fits the observed shortening near supports and at the center diaphragm (Fig. 35) and also greatly improves the agreement for the top fiber.

Approximation to the experimental values by increasing the assumed ultimate creep $\varepsilon_p = 2 \cdot \varepsilon_e$ (p. 72) could not satisfy both the observed top and bottom fiber shortening. The value $\varepsilon_p = 3 \cdot \varepsilon_e$ would result in the identically same predicted strand level curve as shown in Fig. 35 for $\varepsilon_s = 0.0006$, but would have practically no effect on the predicted curve for the top fiber which is nearly free of stress. Thus the test results point to

$$\text{Ultimate shrinkage } \varepsilon_s = 0.0006 \text{ in/in.}$$
$$\text{Ultimate creep } \varepsilon_p = 2.0 \cdot \varepsilon_e$$

as the proper values for the test beam. Both values are in the commonly recommended range for air-cured members.*

The assumed rate of increase of the creep and shrinkage shortening (Fig. 43) agrees very well with the observed combined average values, Fig. 36. Time is the decisive factor rather than the number of design load repetitions. The 100,000 overload cycles did, however, have a definite increasing effect on the fiber shortening as they had on deflections (p. 17), cracks (p. 22), and concrete bending stresses (Table 4).

The assumed function of creep and shrinkage progression as shown in Fig. 43 could well be simplified by using a straight-line variation on a logarithmic time scale, especially since Fig. 36 shows a more rapid initial shortening than predicted.

The concrete fiber shortening at the strand level discussed above causes a loss in prestress progressing with time as shown in Fig. 37. The lower curve gives the predicted steel stress for the unloaded beam as a function of time. The strands were stressed on the bed to 124,600 psi. At release the elastic shortening of the beam caused a computed loss of 8300 psi or 6.7% (p. 72) leaving 116,300 psi (Fig. 37). The subsequent gradual loss due to creep and shrinkage is shown in the figure for the duration of the testing period and is in excellent agreement with the experimental values obtained from Fig. 36. This agreement gives confidence in the predicted final losses which are tabulated below.

PREDICTED FINAL LOSSES IN STEEL STRESS

Loss progression, see Fig. 43. Remain steel stress, see Fig. 37. Calculation of losses, see Appendix	LOSSES			STRESS
	psi	% of f_{si}	% of f_{so}	psi
Initial strand stress f_{si}				f_{si} = 124,600
Elastic loss Δ_e	8300	6.7	7.1	f_{so} = 116,300
Creep loss $\Delta_p = 2 \cdot \Delta_e$	16600	13.3	14.3	
Shrinkage Loss $\Delta_s = 0.0003 \cdot E_s$*	8300	6.7	7.1	
Creep & shrinkage loss	24900	20.0	21.4	f_{se} = 91,400
Total Loss Δf_s	33200	26.7	28.6	91,400

*$0.0006 \cdot E_s$ more correct for test beam.

For design purposes a separate evaluation of loss from each source as shown above is recommended since this is easily done and obviates part of the uncertainty encountered by assuming lump percentages without regard to steel eccentricity, concrete prestress, and curing conditions.

b) Working Load:

In a fully prestressed section or an uncracked partially prestressed section the steel stress increase due to design live load is not affected by losses in prestress. For such homogeneous behavior the steel stress change is $n = E_s/E_c$ times the stress change in the surrounding concrete. Thus the experimental design live load would have caused a predicted steel stress increase of 6500 psi immediately after release, and 6120 psi at the time of the first static test as shown by the upper curve in Fig. 37.

*See for example, loc. cit., p. 20, and Deutsche Normen, DIN 4227, VORGESPANNTE STAHLBETON-TEILE Entwurf April 1950, p. 9.

The test beam, being only partially prestressed, cracked during the first application of design live load. The steel stress then experiences an immediate increase, taking over the lost tension in the lower concrete fibers. From now on the design live load steel stress increases with the loss in prestress as indicated by the distance between the two predicted curves in Fig. 37.

The steel stress increase due to live load after cracking is predicted on the assumption of homogeneous behavior up to the crack-opening load (p. 77). The additional steel stress due to loading beyond the crack-opening load is assumed to equal the total tension that the concrete would carry if still uncracked. This simplified method of analysis is easy and, as shown by the comparison with observed behavior (Fig. 37), sufficiently accurate and on the safe side even up to 40% above crack-opening load (8. Static Test). The accuracy of this method becomes poorer as the load increases, giving increasingly too high steel stress.

The observed steel stress increase due to the first application of design live load (Fig. 37) indicates that the cracking load is just exceeded, as confirmed by inspection (Fig. 33) and by bottom fiber strain measurements (Fig. 36). The subsequent three static tests performed during the first million load repetitions show a marked increase in live load steel stress from about 7000 psi to about 11,000 psi, approaching the predicted value 11,000 psi at the time of the 4. Static test. The additional time and 300,000 design load cycles resulted in a smaller live load effect which at the 7. Static test (Fig. 37) had dropped to about 9000 psi. The final 100,000 overload cycles again increased the design live load steel stress change to 10,700 psi through their increasing effect on prestress loss. However, the live load effect did not again approach the predicted level. Thus it appears that the design load repetitions first tended to increase the steel stress towards the predicted value, but later brought about the opposite effect. An explanation is offered below under "Cracking Load." However, the water-proofed SR-4 gages which yielded this information cause a destruction of bond over about 4 in. length, and the live load stress in un-disturbed strands may therefore be larger than those observed.

For completeness Fig. 37 also shows the predicted final prestress of 91,400 psi and the corresponding design live load effect of 17,000 psi, which add up to a total steel stress under design load after all losses of 108,400 psi. The steel stress due to design live load, were all prestress lost, would have been 64,500 psi (p. 77). One important point often mentioned is clearly demonstrated in Fig. 37: The initial stress in the steel on the pouring bed was never again reached under the full design load. For the test beam this statement would also hold had the beam been post-tensioned since the steel stress immediately after release (elastic loss deducted) was as large as the stress at any subsequent stage.

The observed variation along the beam of the steel stress change due to design live load is plotted in Fig. 38. The predicted stress patterns for the un-cracked stage (First Static test) and after the design and overload repetitions (8. Static test) are shown. Over the un-cracked parts of the beam towards the supports the agreement is very good and the variation with age and number of load repetitions is small. Over the cracked center region the steel stress change varied as just discussed above and never reached the predicted value considering cracking and prestress losses up to the 8. Static test.

c) Cracking Load:

The steel stress increase is shown in Fig. 39 as a function of the load at each third-point. The corresponding moment may be obtained by multiplying the load by the distance 12 ft. from the support to the load point.

Opening of cracks at the bottom fiber is indicated by an appreciable deviation from the initial slope of the curves in Fig. 39. These crack-opening loads at various ages are plotted in Fig. 33 and agree fairly well with predictions.

A fully prestressed member would experience a linear steel stress increase as indicated in Fig. 39. The agreement with the observed behavior is satisfactory until the predicted crack-opening load is approached. This load is reduced by losses in prestress (p. 76) and the corresponding steel stress is proportional to $n = E_S/E_C$; thus the separate predicted curves for the first and the 9. Static tests, at the outset and the end of testing period, respectively.

The predicted additional steel stress after cracking is computed as described above under "Working Load" and agrees satisfactorily well with the observed behavior up to the design live load. At higher loads the predicted curves approach the slope of the curve shown (Fig. 39) for non-prestressed behavior and result in conservative stress estimates. However, the method combines simplicity with reasonable and safe results. The alternative simplifying assumption of non-prestressed behavior after crack-

opening (Method c, p. 77) would result in a line leaving the crack-opening point at the slope indicated in Fig. 39, and thus give considerably poorer steel stress values.

The steel stress across a crack will initially be appreciably larger than in regions between cracks which are partially relieved of strain consumed by the cracks. The steel stress difference is transferred to the concrete over a certain bond length next to the cracks which occurred with an average spacing of about 8 in. A large number of load repetitions may be expected to wear down this bond and thus increase the interior bond length required. The bond length is also known to increase with time due to concrete creep effects. Such internal bond readjustment over short lengths adjacent to the cracks distributes the crack steel strain over a larger length and consequently reduces the peak steel stress. Over the outer thirds of the test beam, having a moment gradient, internal bond readjustment will progress from the load points towards the supports thus reducing the average steel stress due to the load between load points. This effect may explain the reduction in live load steel stress at a large number of load repetitions as discussed earlier in connection with Figs. 37 and 38. Noises characteristic for sudden bond failure were distinctly heard during the first application of 54% overload but were not accompanied by any end slip of the strands. This observation tends to confirm the above assumption of internal bond readjustment which also explains the strand behavior during the destruction test.

As a consequence, bond anchored prestressed steel in continuous structures should terminate at points of small live load moment.

d) Ultimate Load:

The steel strains at four locations along the beam were observed during the third-point and center-load destruction tests and are shown in Fig. 40. In contrast to the previous figures individual strain gage readings are plotted. The final moment increase produced by center loading is for convenience represented in Fig. 40 in terms of equivalent third-point load. Considering the prestress the shown strain values are proportional to the steel stress up to 3800 micro-in/in. (E_s = 27,300,000 psi) which includes most of all the figure.

The gage group A, only one foot from the support, should show no strain increase and actually give values very close to the zero abscissa. Thus, since no end slip occurred, the internal bond failure did not reach to the supports. Group D located 1'-9" from the other support confirms this finding.

Group B, 5'-7" from the support, largely follows the predicted increase. However, gage B20 in the lower strand row behaved strangely at about 55 kip load or 1.28 times the crack-opening load at this location. This may indicate internal bond readjustment but could be failure of the glue joining the gage to the strand. Such behavior is quite pronounced for two of the four C-group gages near mid-span, both are in the lower strand row which in a severely cracked member will most likely suffer bond destruction. The predicted steel strain at failure was 10,900 micro-in/in. which was not reached by any of the gage-carrying strands. The predicted ultimate load, however, was exceeded by 9% (Table 3) which points to a higher average ultimate load stress in the 40 strands than indicated by the four carrying strain gages at the center.

6. Diagonal Tensile Stresses

a) Release of Prestress:

The far most dominating effect on the stress distribution near the ends of the beam is the prestressing force which is transferred to the concrete over a rather short distance from the end face. Thus the predicted principal stresses near the support (p. 75) is practically identical to the prestress pattern as shown in Fig. 41. The experimental values given in this figure are obtained from SR-4 rosette strain gage readings (Figs. 14, 15). Although the detail agreement with the computed values is poor the general predicted behavior is verified.

At the strand level the principal stresses are nearly horizontal as predicted. The first lower gage 1'-6" from the beam end show 1050 psi horizontal compression on the one side and 1220 psi on the other as compared to 1190 psi predicted. This indicates that the required initial end bond anchorage length was less than 1'-6" or 180 times the wire diameter.

Near the top the observed tensile strains at release are appreciably larger than predicted (Fig. 41) which is probably due to cracking which took place at this stage (Figs. 26, 27). Such cracking lowers the neutral axis which again is indicated by the observed stress pattern in Fig. 41.

b) Working Load:

The maximum predicted principal stresses at the supports under full design load were 560 psi compression and 50 psi tension near mid-depth at the start of the hollow section (p. 75). The prestress alone caused 507 psi compression at this location, and the change due to live load was too small to be checked by SR-4 strain gage readings.

c) Ultimate Load:

The total maximum diagonal tension near the supports at predicted ultimate load was only 285 psi and no diagonal cracks occurred. The predicted separate effect of the ultimate live load was 400 psi tension and compression at 45° near mid-depth of the hollow section. The few strain gage readings obtained near the ultimate load (Fig. 42) confirmed the predicted direction of the two principal stresses, but the maximum observed magnitude was only 320 psi.

E. CONCLUSIONS

A 38-ft pretensioned concrete highway bridge beam containing 40 bonded 5/16 in. diameter strands has been subjected to a magnitude (H20-S16-44) and number (1,300,000) of loadings and overloadings (100,000 repetitions of 54% overload) that amply cover the lifetime service of such a member in a most severe bridge location.

The results of this test are summarized below together with some recommendations for improvement of manufacturing.

General

1. The beam proved to be structurally entirely satisfactory for its intended purpose.
2. The methods of analysis used to predict the beam behavior (see Appendix) are satisfactorily accurate or on the safe side.
3. The beam satisfied the current Pennsylvania Department of Highway's recommendations (p. 80) for such members with the exception that a higher prestress should be applied. The partial prestress used in the test beam caused more severe testing conditions than those actually experienced for fully prestressed members. The cracking load should be computed on the assumption that the concrete carries no tensile stresses, and should not be less than the design load.

Materials

4. The concrete just met the required cylinder strength of 3300 psi at transfer of prestress and 5000 psi at 28 days. The final modulus of elasticity is about 4,000,000 psi. A 6000 psi concrete with corresponding higher allowable stresses could economically be obtained without appreciable compacting difficulties by pouring a dryer mix. A more plastic mix for covering the strands should be obtained by reducing the aggregate content rather than by increasing the water content.
5. The seven-wire 5/16 in. diameter time-temperature treated strand with ultimate strength of 275,000 psi and modulus of elasticity of 27,700,000 psi (Fig. 18) has entirely satisfactory bond properties for this application.

Beam Behavior

6. Deflections:
   a) The deflections under design live load agreed closely with the predicted (0.54 in. = L/800) and were little affected by the repeated loading but increased 30% due to the overload cycles (Fig. 20).
   b) The design live load and overload repetitions caused a permanent deflection about equal to the initial camber produced by prestressing.
   c) Loading to within nine-tenths of the destruction load caused a permanent deflection of 1/200 of the span length (Fig. 21).
   d) The deflection under 91% of the ultimate moment produced by third-point loading was 9.6 in. (Fig. 21). The deflection at failure produced by center loading was 11.5 in. (Fig. 24).
7. Slip:
   a) No end slip of the strands indicating end bond failure occurred at any stage of the test.
   b) Interior bond readjustment due to load repetitions (Figs. 37, 38) and high static overload (Fig. 40) is indicated but was not detrimental to the beam behavior.
8. Cracking:
   a) The test beam was only partially (70%) prestressed and cracked during the first loading at a load

indicating little effect of concrete tension. (Figs. 33, 37).

b) It is recommended that the cracking load be computed on the basis of zero bottom fiber stress.

c) The length, width and number of cracks were extended by design load and overload repetitions. (Figs. 26, 27).

9. Concrete Stresses:

a) The concrete stresses at release and due to design live load computed by conventional methods are satisfactorily accurate (Figs. 31, 32, 41, 42).

b) The compressive concrete bending stresses due to design live load were little affected by design load repetitions but increased by about 25% due to the overload cycles (Table 4).

10. Prestress Losses:

a) For design purposes a separate evaluation of loss from each individual cause (elastic shortening, creep, shrinkage, etc.) is recommended as this is easily done and leads to accurate values (Figs. 35, 37).

b) The observed progressive creep and shrinkage losses are satisfactorily described for the curing conditions of the test beam by assuming ultimate shrinkage 0.0006 in/in. and ultimate creep twice the elastic strain (Figs. 35, 37) increasing linearly to 10 years on a logarithmic time scale (Fig. 43). Under better curing conditions a shrinkage of about 0.0003 in/in. is more likely to be attained.

c) The design live load repetitions did not cause losses in addition to those described above, and the overload repetitions had only a minor loss effect. (Fig. 37).

11. Steel Stresses:

a) Below crack-opening load the live load steel stresses agree closely with the values computed assuming homogeneous cross-section (Fig. 38).

b) The additional steel stress in a cracked section is conservatively estimated with sufficient accuracy by assuming the steel to carry the total tension in the concrete if still un-cracked (Fig. 39). The accuracy of this method decreases with increasing load.

c) The design live load cycles caused steel stress increase as cracking progressed but a decrease as interior bond readjustment developed, so that the live load effect never reached the value predicted as described above (Fig. 37).

d) The initial stress in the steel on the pouring bed was never again reached under the full design load (Fig. 37).

12. Effect of Repeated Loading:

a) The 1,300,000 design load applications caused extension of the crack pattern but had only minor effects on the beam behavior under live load.

b) The 100,000 repetitions of 54% overload were not destructive but left indications of distress.

13. Ultimate Load:

Following completion of the repetitive load test program the beam failed due to crushing of the concrete (Fig. 28) at a maximum moment of $(M_D + 4.2\ M_L)$ or $3.1\ (M_D + M_L)$ which was 9% higher than predicted and 22% higher than the required $2.5\ (M_D + M_L)$. No bond or steel failure occurred. (Table 3).

F. ACKNOWLEDGEMENTS

The work reported was carried out through the Lehigh University Institute of Research under the guidance of the Lehigh Prestressed Concrete Committee of which Mr. A. E. Cummings, is Chairman, representing the Reinforced Concrete Research Council of the Engineering Foundation. This committee representing the sponsors, is composed of the following members, each of whom aided in many ways throughout this study.

Reinforced Concrete Research Council,	Mr. A. E. Cummings
Pennsylvania Department of Highways,	Mr. L. A. Porter
U. S. Bureau of Public Roads,	Mr. Neil VanEenam
John A. Roeblings's Sons Corporation,	Mr. H. K. Preston
American Steel and Wire Div., U. S. Steel,	Mr. W. O. Everling
Concrete Products Company of America	Mr. B. J. Baskin
Lehigh University,	Prof. W. J. Eney

The Research Corporation also aided the sponsors financially in building the cyclic loading machine.

The program was co-directed by Professor W. J. Eney, first with Dr. A. C. Loewer, Jr., during the planning and initial stages, and then with Dr. K. E. Knudsen during the manufacturing, testing, and reporting stages of the investigation. The great amount of work involved in making the test beam, securing and analyzing the test data was carried out with skill and untiring effort by Alexis Smislova, Daniel H. Brown, Jr., Alfred Roesli, Research Assistants; and Cesar A. Buenaventura, Graduate Fellow in the Fritz Engineering Laboratory, Department of Civil Engineering and Mechanics.

The work of Kenneth R. Harpel, Foreman, with his mechanics and technicians, in assisting throughout the test program and in constructing the repetitive loading machine; and Mrs. Veronica Olanovich, project secretary, is highly appreciated.

G. NOMENCLATURE

The following nomenclature used in this report is that recommended by Joint ACI-ASCE Committee 323 as published in ACI Journal, October 1952, with necessary additions.

Cross-sectional constants:

A_c	= area of entire concrete section (steel area not deducted)
A_c'	= area of transformed section $A_c' = A_c + (n - 1) A_s$
A_s	= total steel area, steel area in simply reinforced section
A_sb, A_st	= area of bottom (top) reinforcement in doubly reinforced section
c.g.c.	= center of gravity of entire concrete section
c.g.c.'	= center of gravity of transformed section
c.g.s.	= center of gravity of steel area
h	= total depth of section
d	= effective depth of section
b	= width of rectangular section
b'	= width of web of beam
t_b, t_t	= depth of bottom (top) flange of beam
b_b, b_t	= width of bottom (top) flange of beam
y_b, y_t	= distance of bottom (top) fiber to c.g.c.
y_b', y_t'	= distance of bottom (top) fiber to c.g.c.'
e	= eccentricity of c.g.s. with regard to c.g.c.
e'	= eccentricity of c.g.s. with regard to c.g.c.'
I_c	= moment of inertia of entire concrete section about c.g.c.
I_c'	= moment of inertia of transformed section about c.g.c.'
Z_b, Z_t	= section modulus of bottom (top) fiber, referred to c.g.c.
Z_b, Z_t'	= section modulus of bottom (top) fiber, referred to c.g.c.'
r	= radius of gyration
n.a.	= neutral axis of cracked section

Loads:

w_G	= dead load per unit length when the prestress is being established (dead load of prestressed girder)
w_S	= additional (superimposed) dead load per unit length applied when the prestress has been established (dead load of deck, flooring, roadway, etc.)
w_D	= total dead load per unit length = $w_G + w_S$
w_L	= distributed live load per unit length
P_L	= concentrated live load
M_G	= bending moment due to w_G

M_S = bending moment due to w_S

M_D = bending moment due to w_D

M_L = bending moment due to live load

M_e = bending moment due to eccentricity of prestress force

V = shear

$\delta \frac{L}{2}$ = deflection at center of span

$\delta \frac{L}{4}$ = deflection at quarter point of span

m = multiple of live load moment including impact

m' = multiple of total maximum design moment

Q'_c = lst. moment of area above c.g.c.'

Notation relating to prestress only:

First loading stage-Combined action of prestressing forces and dead loads (sustained loads)
Second loading stage-Combined action of prestressing forces, dead loads and live loads
Third loading stage-Ultimate loads based on cracked tension zone

F_i = initial prestress force

F_o = prestress force after release

F = effective prestress force after deduction of all losses

Stresses:

Concrete----

f'_c = cylinder strength at 28 days

f'_{ci} = cylinder strength at the age of prestressing

f_{cp} = permissible compressive stress

f_{cpi} = permissible compressive stress at the age of prestressing

f_c = compressive stress generally

f_c^s = stress at c.g.s.

f_c^c = stress at c.g.s.

f^b_{Fi}, f^t_{Fi} = stress at bottom (top) fiber due to initial prestressing only

f^b_F, f^t_F = stress at bottom (top) fiber due to effective prestressing only

f^b_G, f^t_G = stress at bottom (top) fiber due to dead load w_G only

f^b_S, f^t_S = stress at bottom (top) fiber due to dead load w_S only

f^b_D, f^t_D = stress at bottom (top) fiber due to total dead load w_D only

f^b_L, f^t_L = stress at bottom (top) fiber due to live load only

f^b_{FoG}, f^t_{FoG} = stress at bottom (top) fiber due to prestressing at release, F_o, and dead load w_G

f^b_{FG}, f^t_{FG} = stress at bottom (top) fiber due to effective prestressing F, and dead load w_G

f^b_{FD}, f^t_{FD} = stress at bottom (top) fiber due to effective prestressing F, and total dead load (stresses at first loading stage)

f^b_{FT}, f^t_{FT} = stresses at bottom (top) fiber due to effective prestressing, F, and total load (stresses at 2nd. loading stage)

f_{cu} = compressive stresses at failure (3rd. loading stage)

f_t = tensile stress generally

f_{tp} = permissible tensile stress

v = shearing stress

S_c = principal compressive stress

S_t = principal tensile stress

S_x = vertical stress component

S_y = horizontal stress component

E_c = modulus of elasticity of concrete

n = ratio of modulus of elasticity of steel, E_s, to that of concrete, E_c

Steel----

f'_s = ultimate strength of steel

f_{sp} = permissible tensile stress

f_s = steel stress generally

f_{si} = steel stress due to initial prestressing

f_{so} = steel stress due to prestressing after release

f_{se} = steel stress due to effective prestress force after deduction of all losses

Δ_e = steel stress loss due to elastic deformation of concrete

Δ_s = steel stress loss due to shrinkage

Δ_p = steel stress loss due to creep of concrete

Δt = steel stress loss due to creep in steel

Δf_s = total steel stress reduction

f_{sb} = additional bending stress in cracked section

f_{su} = stress at failure

E_s = modulus of elasticity of steel

f_{sL} = increase of steel stress due to live load

H. REFERENCES

1. Mayo, Lore, Loewer and Eney, Progress Report No. 1, A COMPARISON BETWEEN ORDINARY REINFORCED AND PRESTRESSED REINFORCED CONCRETE BEAMS, January, 1952
2. Mayo, Loewer and Eney, Progress Report No. 2, TEST OF A PRETENSIONED CONCRETE BEAM CONTAINING 5/16" DIA. BONDED STRANDS, June, 1952.
3. Smislova, Loewer and Eney, Progress Report No. 3, REPORT ON A PRE-TENSIONED PRESTRESSED CONCRETE BEAM, May, 1952.
4. Smislova, Loewer and Eney, Progress Report No. 4, STRESS DETERMINATION IN STEEL STRAND BY SR-4 GAGES April, 1952, Published in PRODUCT ENGINEERING, April, 1953, p. 214.
5. FACTORIES FOR PRESTRESSING: BIG BUSINESS IN PENNSYLVANIA Engineering News-Record, January 15, 1953, p. 35.
6. CONCRETE PAVEMENT DESIGN, Portland Cement Association, Chicago, 1951.
7. T. B. Dimmick, Highway Transport Research Branch, U.S. Bureau of Public Roads, TRENDS IN TRAFFIC VOLUMES, VEHICLE TYPES AND WEIGHTS "Public Roads," Vol. 27, No. 6, February 1953, p. 111.

J. TABLES AND FIGURES

TABLE 1. CONCRETE MIX DATA

	CONCRETE COVERING STRANDS	CONCRETE ABOVE STRANDS	
	Before Vacuuming	Before Vacuuming	After Vacuuming
MIX PROPORTIONS			
Cement	908 lbs/cu. yd.	918 lbs/cu yd.	962 lbs/cu. yd.
Water	322 "	318 "	304 "
Sand	1029 "	1040 "	1088 "
Gravel	1620 "	1640 "	1716 "
Sum	3879 lbs/cu. yd.	3916 lbs/cu. Yd.	4070 lbs/cu. yd.
CEMENT-WATER RATIO			
c/w	2.82	2.88	3.16
w/c	0.355	0.347	0.317
Water	4.00 gal/bag	3.90 gal/bag	3.54 gal/bag
AIR CONTENT			
Air Meter	6.3%	4.2%	--
Computed	5.5%	4.9%	--
CONSISTENCY			
Slump	5.5 in.	4.5 in.	--
REMARKS	Ave. for 2 batches	Ave. for 3 batches	For orientation only.

TABLE 2. CONCRETE QUALITY TESTS

AGE (days)	EVENT	MODULUS OF ELASTICITY (1)	COMPRESSIVE STRENGTH (2)	
		Main Concrete (ksi)	Bottom Conc. (psi)	Main Conc. (psi)
5	Day after release	3310(4) 3340(5) 3330	---	3250 3250 3250(3)
32	1. Static Test	3300(4) 3560(5) 3480	3890	(3320) 4890 4890
59	2. Static Test	3430(4) 3740(5) 3590	4470	5010 5970 5490
80	3. Static Test	3480(4) 3750(5) 3620	3940	4690 6160 5430
91	4. Static test	3740(5)	4770	5390 5730 5560
161	Destruction Test	3920(5)	5300	5840 5840 6040 6150 5970
161	Destruction Test	4720(2)		

(1) 6" x 12" cylinders, air cured.
(2) 6" x 12" cylinders, air cured for 33 days, moist cured thereafter.
(3) Moist cured throughout.
(4) Same cylinder.
(5) Same cylinder.

TABLE 3. DESTRUCTION TEST DATA

	THIRD-POINT LOADING[1]			CENTER LOADING		
	Observed	Predicted	%	Observed	Predicted	%
Live load (kips)[2]	62.0	63.7	97	92.9	85.2	109
Live load Moment (in. k.)[2]	8950	9185	97	10,040	9185	109
Total Moment (in. k.)	9967	10,200	98	11,057	10,200	108
Deflection (in.)	9.68	9.40	103	11.5	--	--
$M_D + m \cdot M_L$	m = 3.71	3.81	--	m = 4.17	3.81	109
$m' (M_D + M_L)$	m' = 2.81	2.87	--	m' = 3.11	2.87	108

(1) Failure was not obtained
(2) Equivalent weight of surfacing included.

TABLE 4. TOP FIBER STRESS AND BOTTOM FIBER STRAIN IN CONCRETE AT CENTERLINE DUE TO DESIGN LIVE LOAD

STATIC TEST		TOP FIBER STRESS				BOTTOM FIBER STRAIN				
No.	After Cycles	SR-4 Gages		Whittemore		Predicted	SR-4 Gages		Whittemore	
		psi	@	psi	%	micro-in/in	micro-in/in	%	micro-in/in	%
1.	1	950	90	1050	99	284	269	95	275	97
2	300,000	1040	98	1080	102	276	319	116	305	111
3	600,000	1100	104	1000	94	268	347	129	280	105
4	1,000,000	1040	98	980	93	265	326	123	300	113
5	1,000,000	1020	96	1010	95	261	314	120	325	124
6	1,300,000	1020	96	1120	105	253	300	119	345	136
7	1,300,000	1000	94	1260	119	252	299	118	350	139
8	1,400,000	1220	115	1420	134	251	406	162	525	209
9	1,400,000	1150	109	1280	121	248	391	158	575	232
Predicted		1060	100	1060	100					

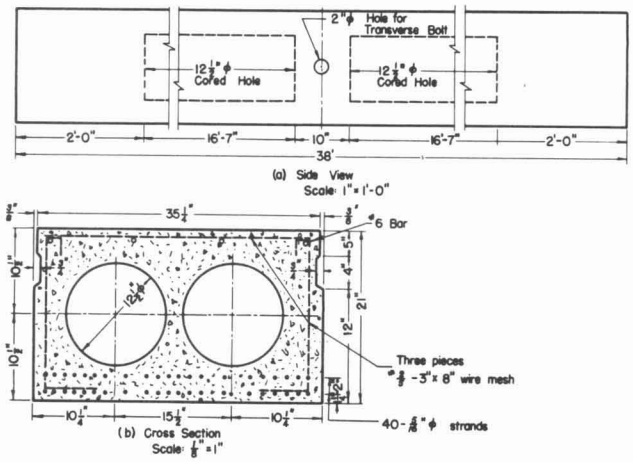

Fig. 1. FIRST FULL-SCALE TEST BEAM

Fig. 2. PRE-TENSIONING OPERATION
The 5/16 " ϕ Strands are Gripped by Strand-vise Fittings and Stressed by Mechanical Jack to 6 5/8"
Elongation Determined by Shim Plates

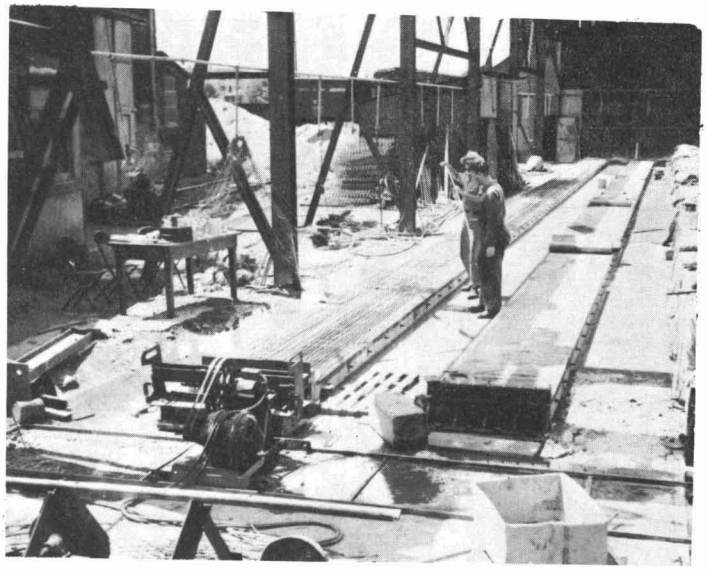

Fig. 3. 120-ft. CASTING BED WITH 40 PRE-TENSIONED 5/16 INCH DIAMETER STRANDS IN PLACE

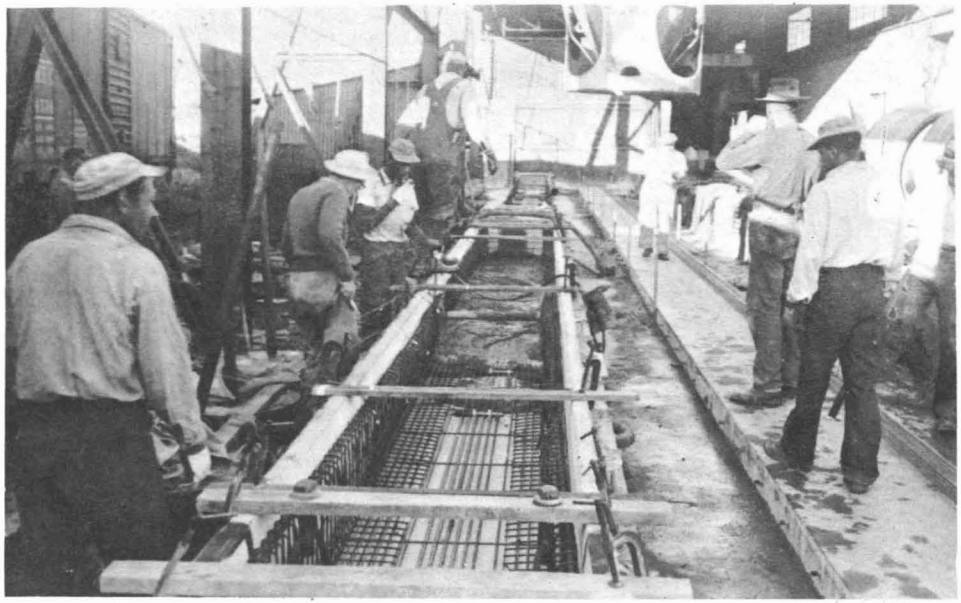

Fig. 4. POURING OPERATION STARTED

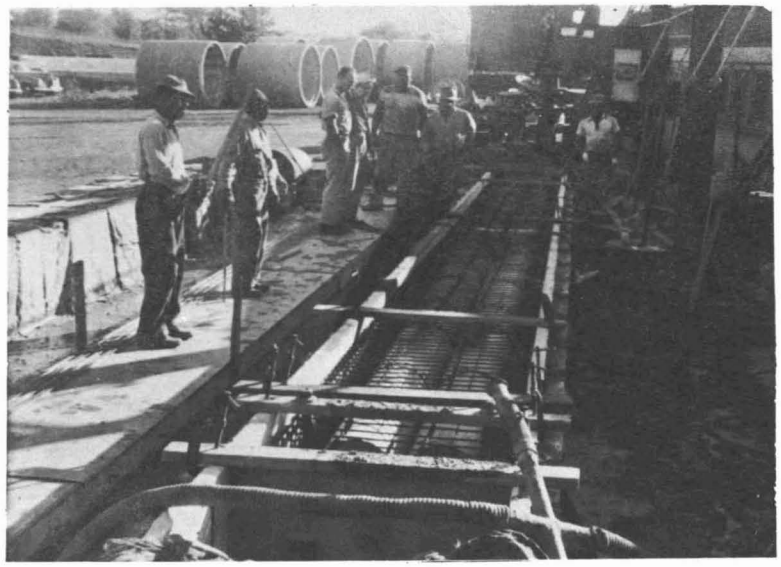

Fig. 5. PAPER TUBES AND TOP WIRE MESH IN PLACE FOR POURING TO CONTINUE

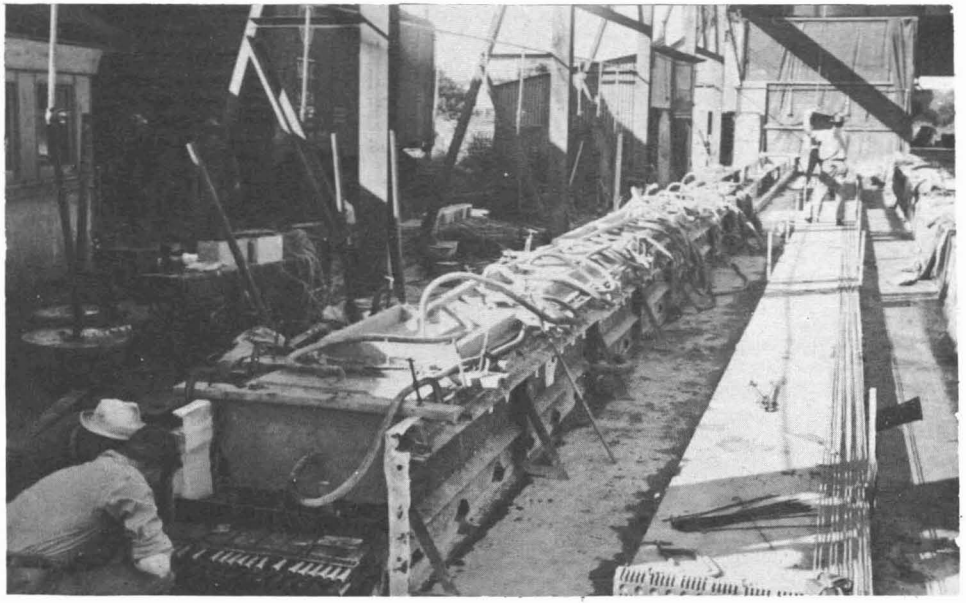

Fig. 6. VACUUM TREATMENT OF TEST BEAM

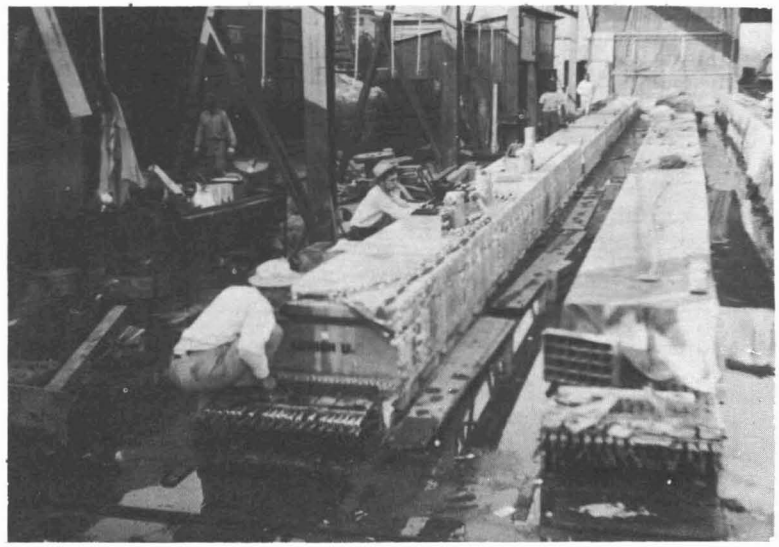

Fig. 7. STRAIN GAGES MOUNTED ON TEST BEAM BEFORE TRANSFER OF PRESTRESS
Other Beams in the Background

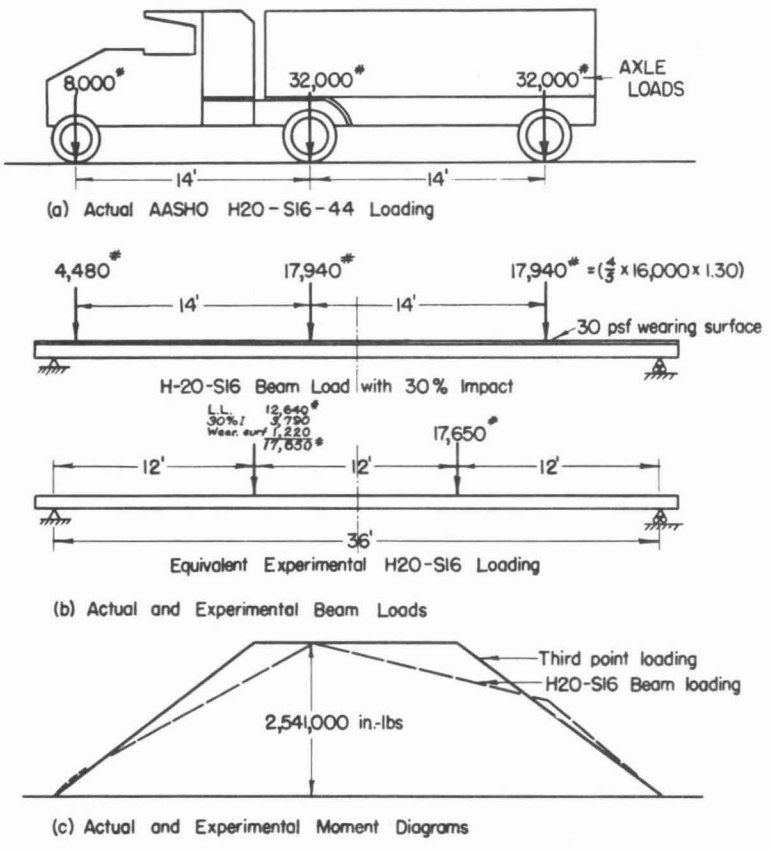

Fig. 8. EQUIVALENT H20-S16-44 TEST LOADING

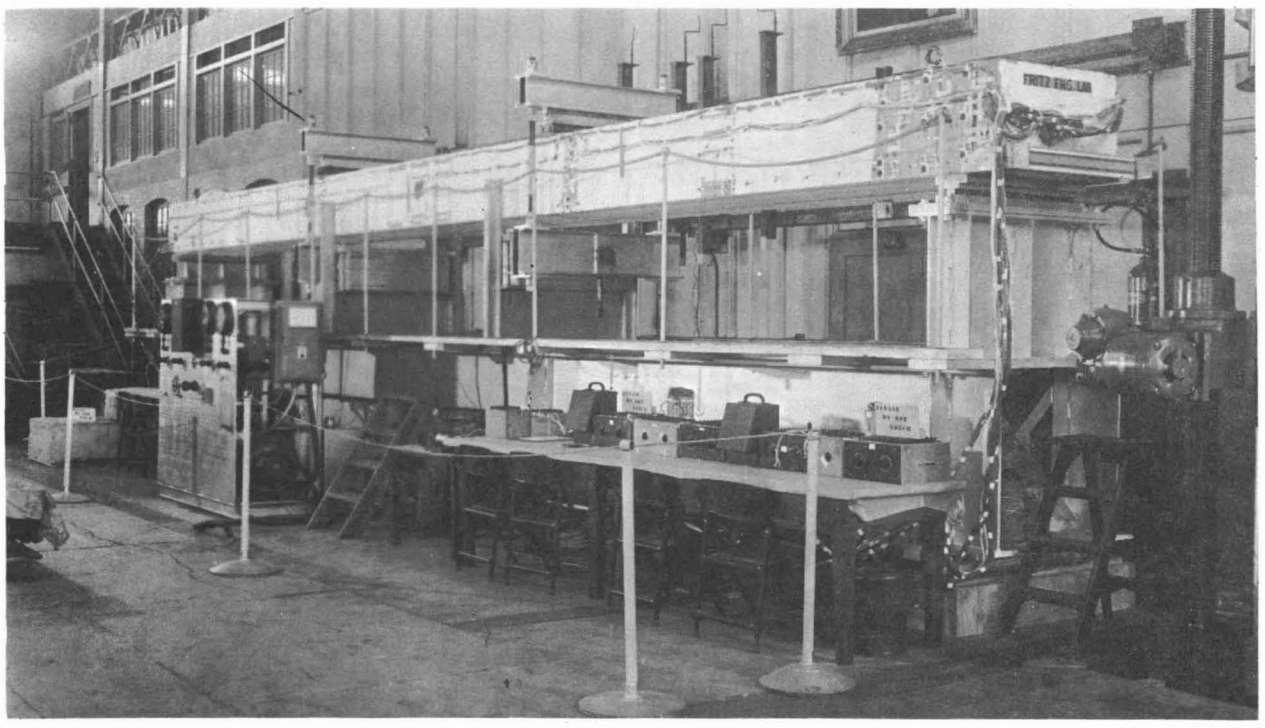

Fig. 9. GENERAL VIEW OF TEST SET-UP

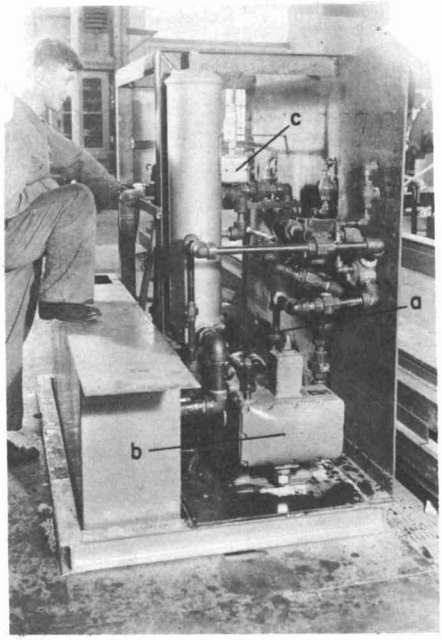

Fig. 10. HYDRAULIC LOADING UNIT

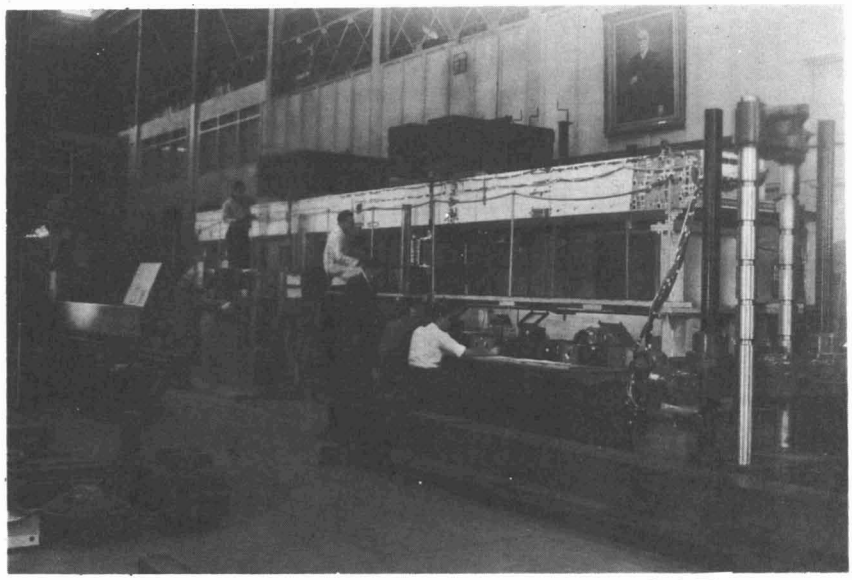

Fig. 12. 6400 lbs. DEAD WEIGHTS AT EACH THIRD-POINT Applied During the 100,000 Overload Repetitions

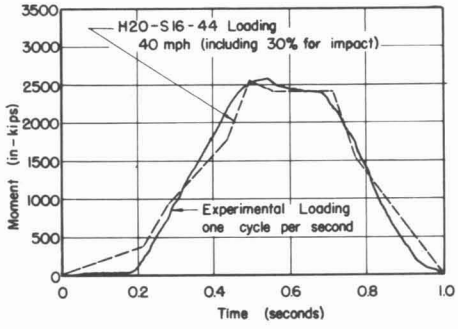

(a) Experimental and Actual Moment-Time Diagram

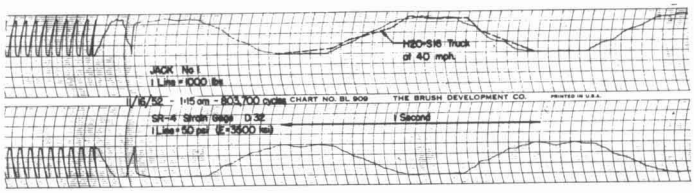

(b) Third Point Loading Recorded by Oscillograph

Fig. 11. MOMENT-TIME DIAGRAMS FOR CENTERLINE BEAM SECTION

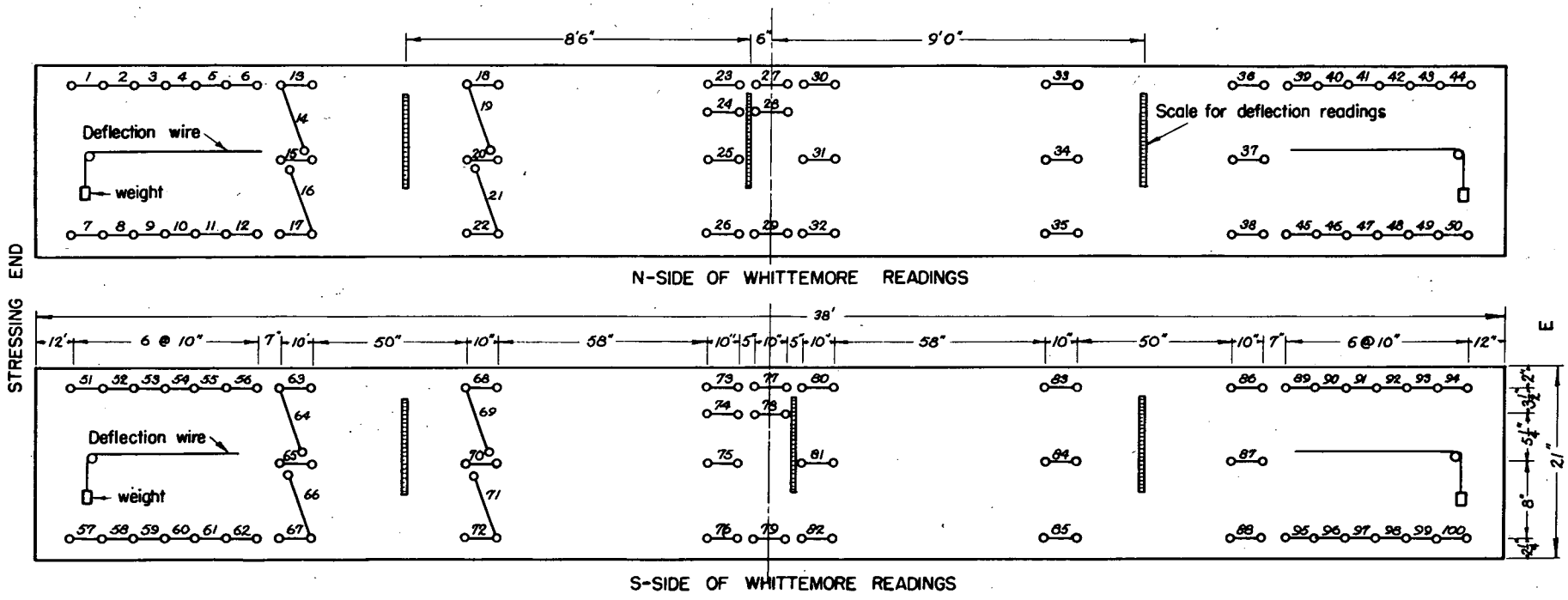

Fig. 13. LOCATION OF WHITTEMORE STRAIN READINGS

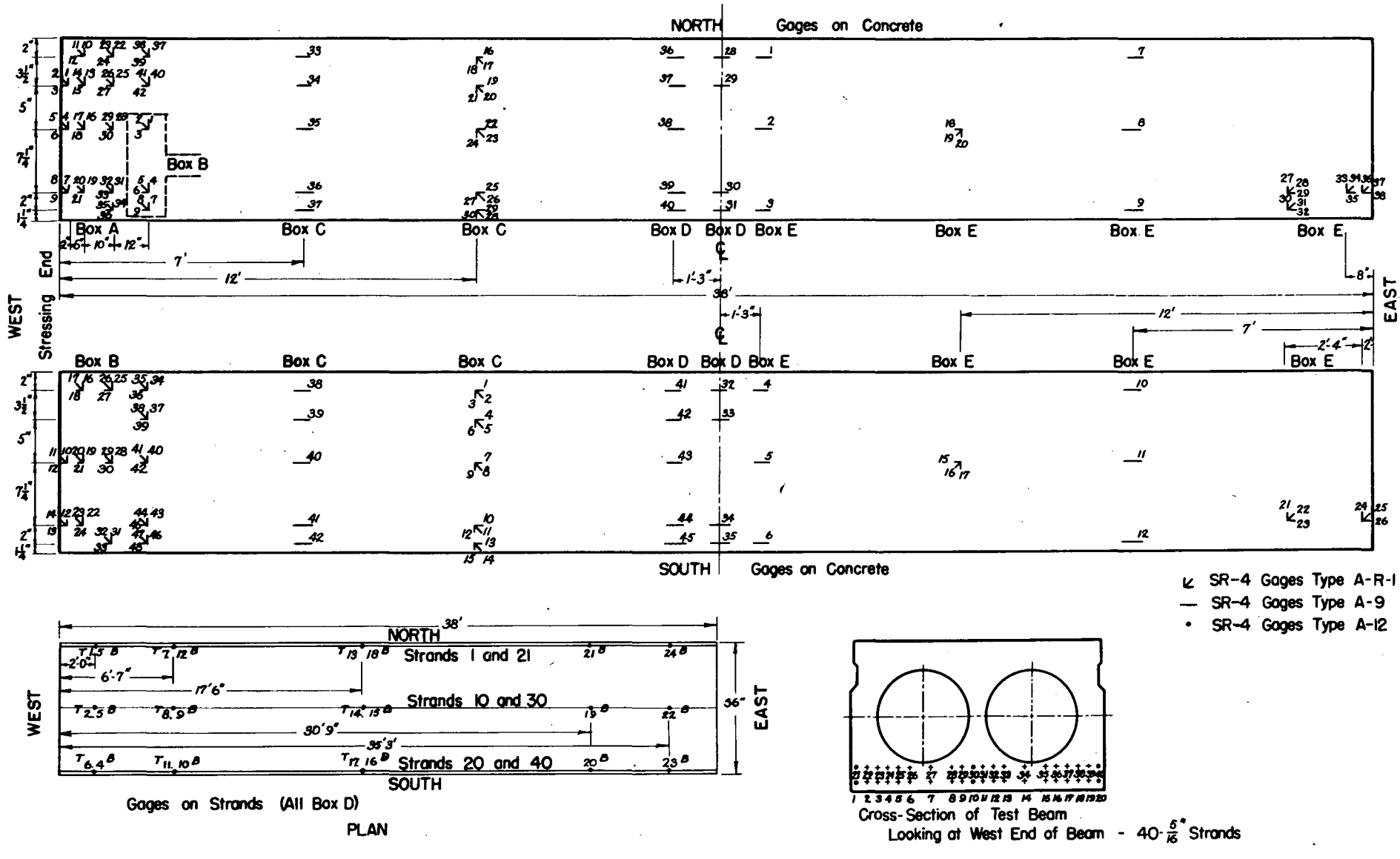

Fig. 14. LOCATION OF SR-4 STRAIN GAGES

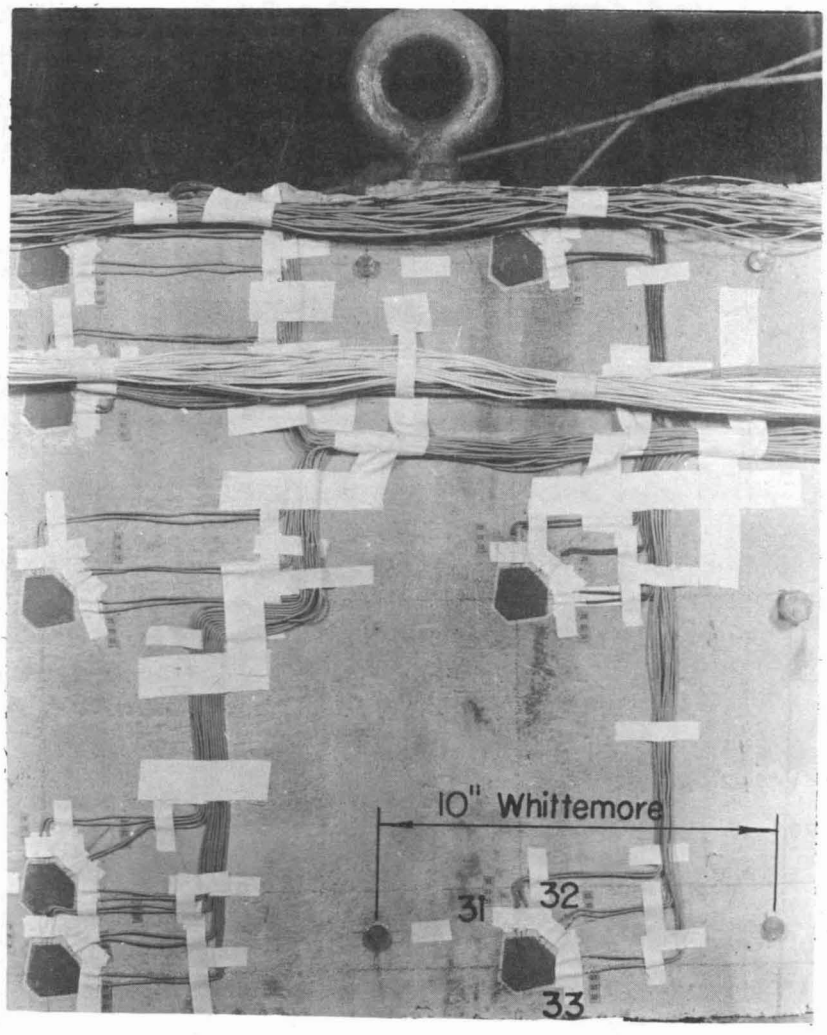

Fig. 15. SR-4 STRAIN GAGES AND WHITTEMORE GAGE POINTS APPLIED TO THE BEAM SURFACE

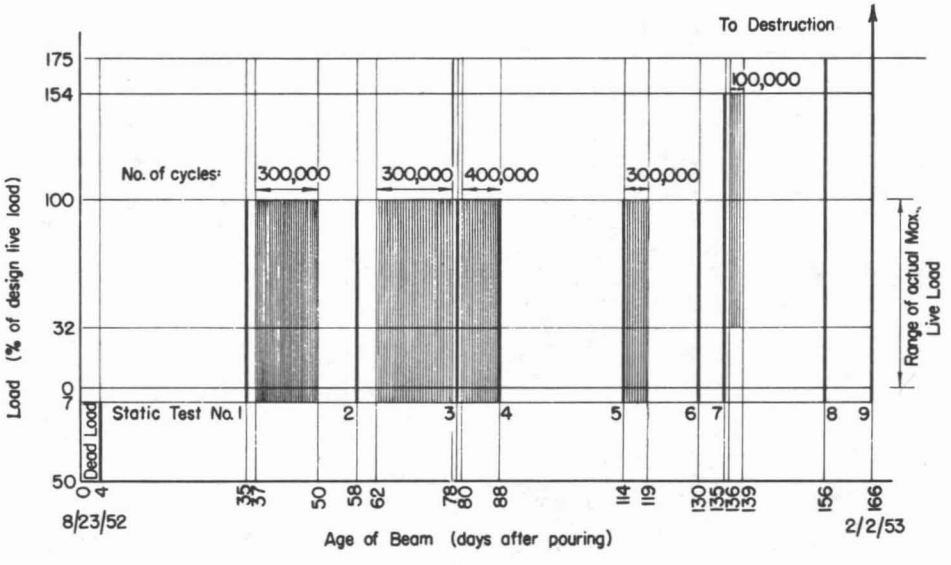

Fig. 16. PROGRAM FOR FIRST FULL-SCALE BEAM TEST

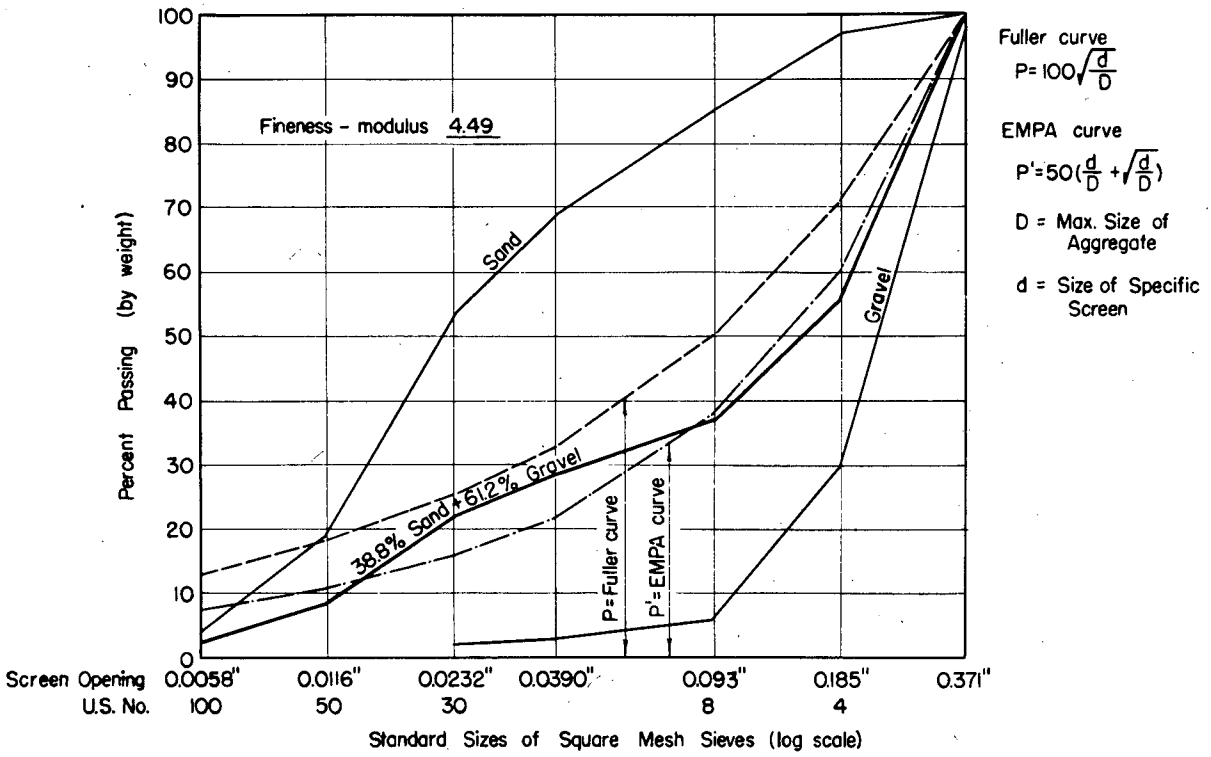

Fig. 17. GRADING OF AGGREGATES USED IN TEST BEAM

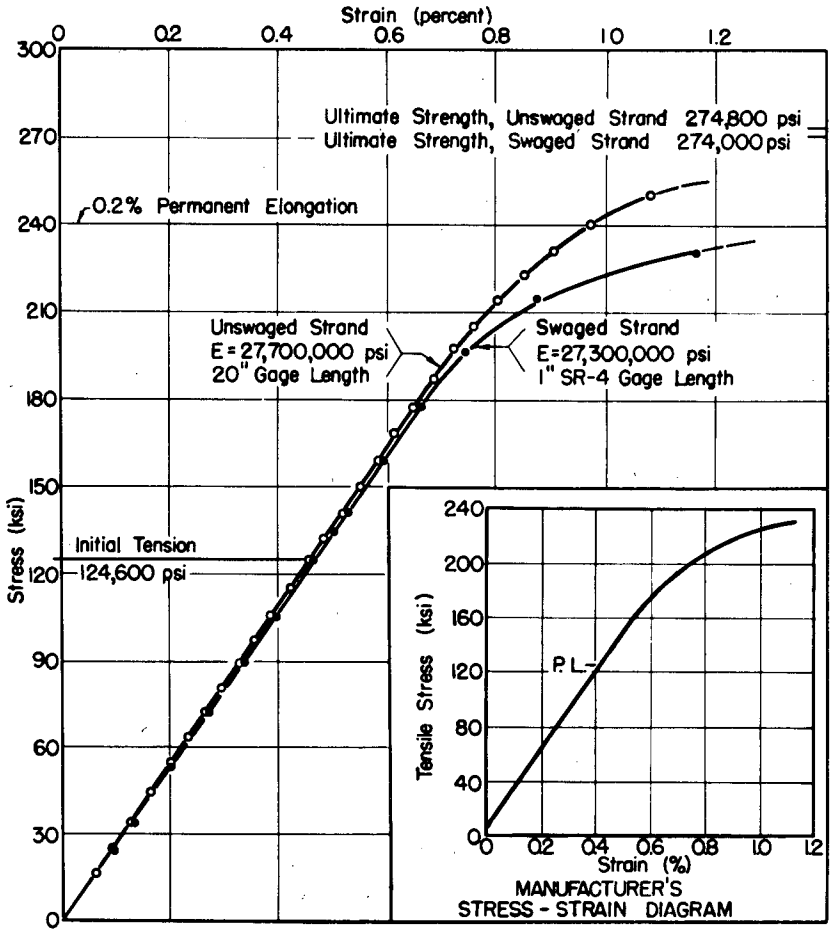

Fig. 18. STRESS-STRAIN DIAGRAM FOR 5/16"
TIME-TEMPERATURE TREATED STRAND

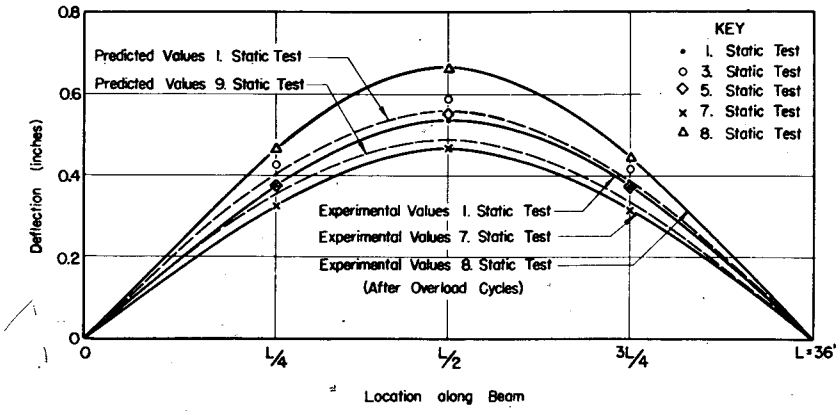

Fig. 19. DEFLECTIONS DUE TO DESIGN LIVE LOAD

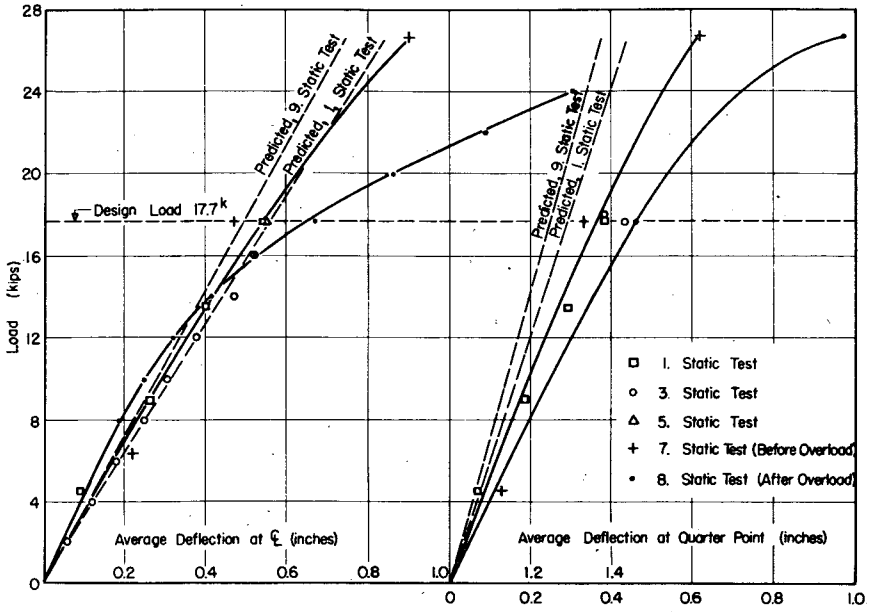

Fig. 20. LOAD-DEFLECTION RELATION AT CENTERLINE AND QUARTERPOINTS

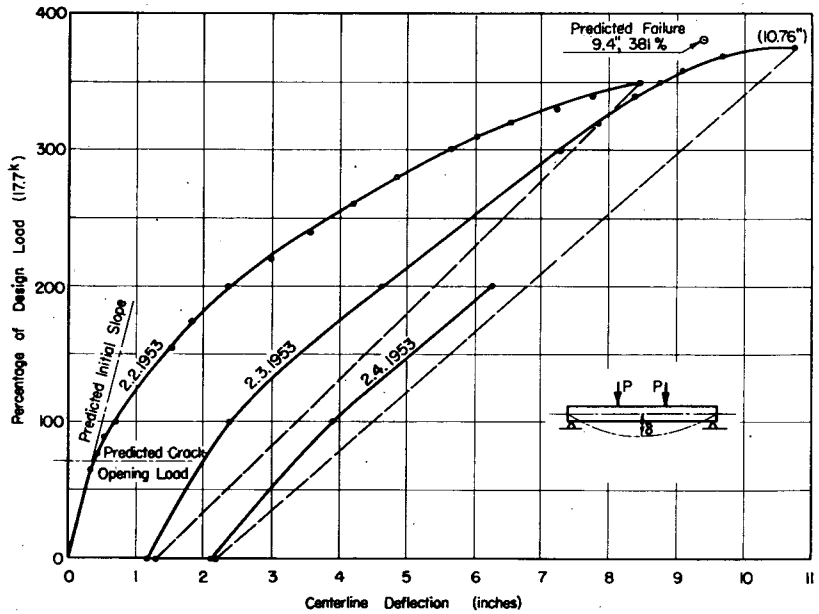

Fig. 21. DESTRUCTION TEST LOAD-DEFLECTION DIAGRAM

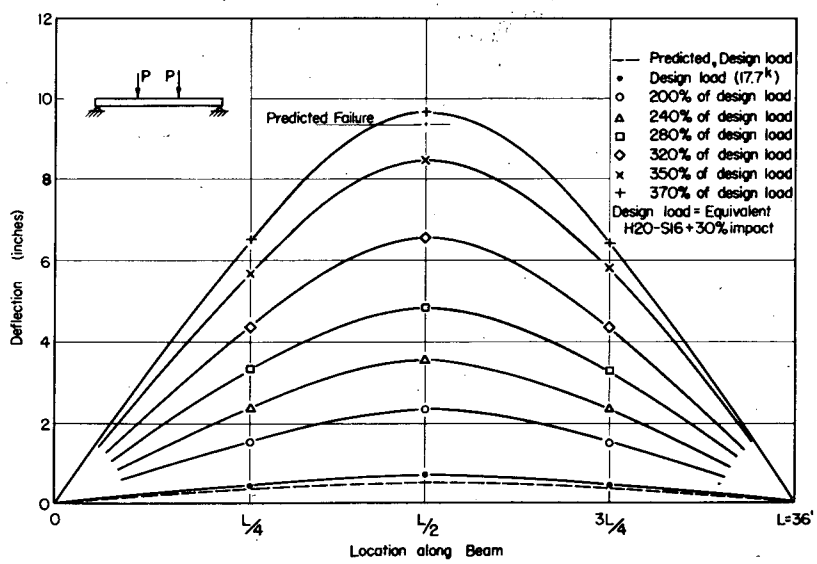

Fig. 22. DEFLECTED SHAPE DURING DESTRUCTION TEST

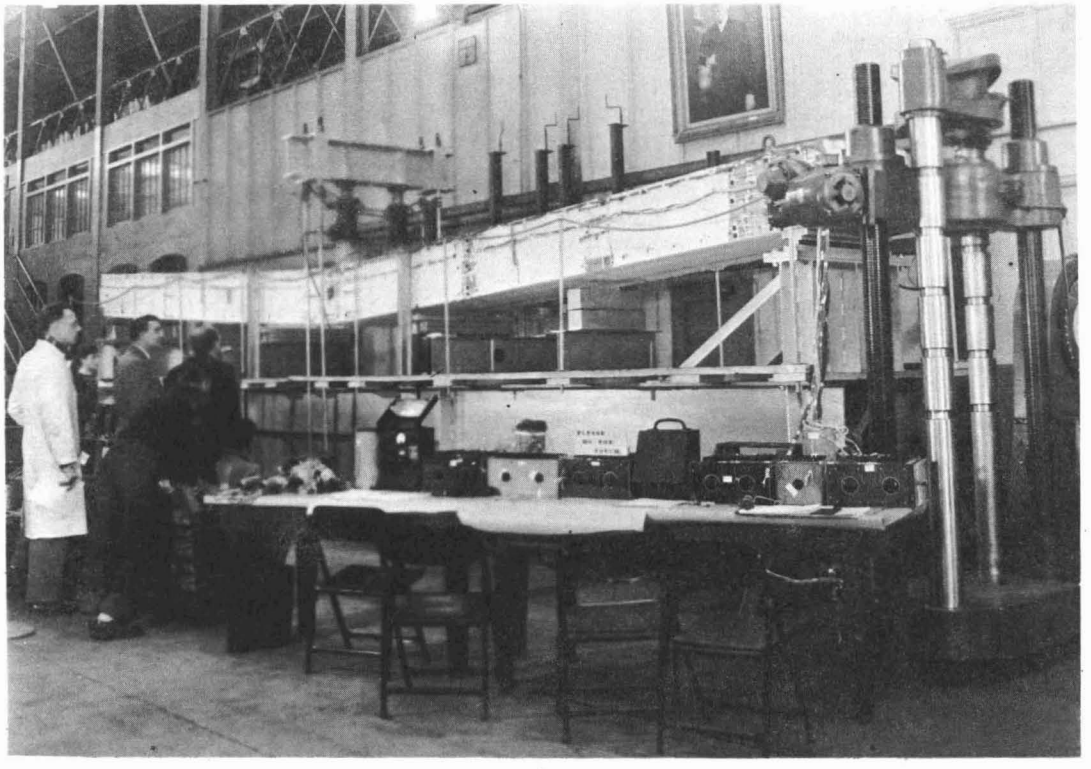

Fig. 23. BEAM IMMEDIATELY BEFORE FAILURE

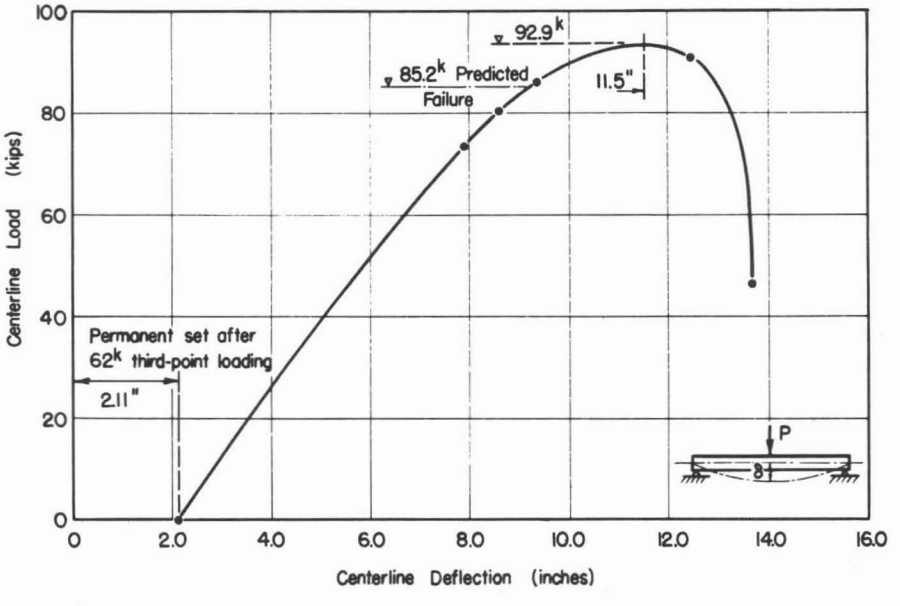

Fig. 24. CENTERLINE DEFLECTION DURING DESTRUCTION TEST

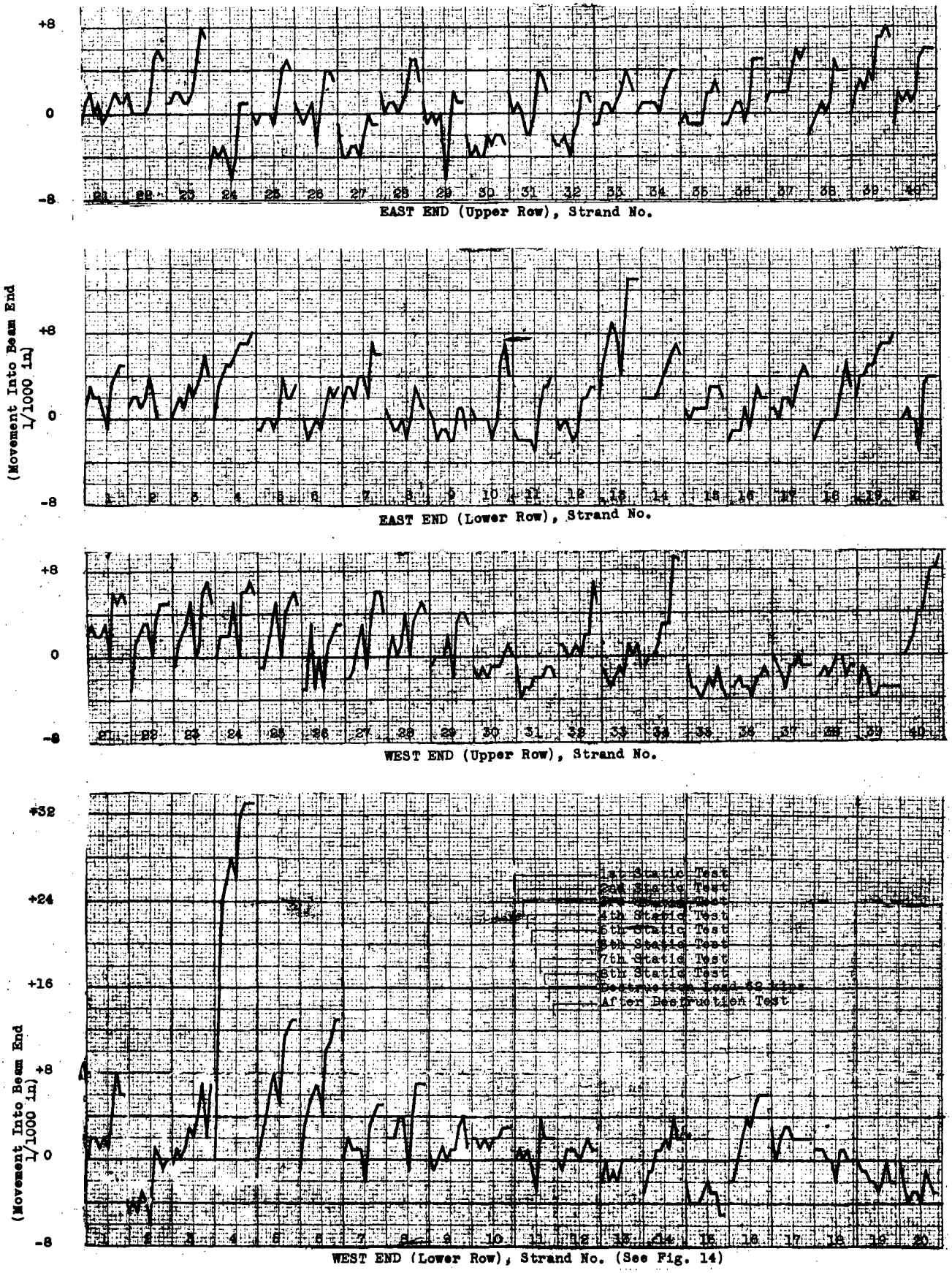

Fig. 25. LOG OF MOVEMENT OF ENDS OF STRANDS

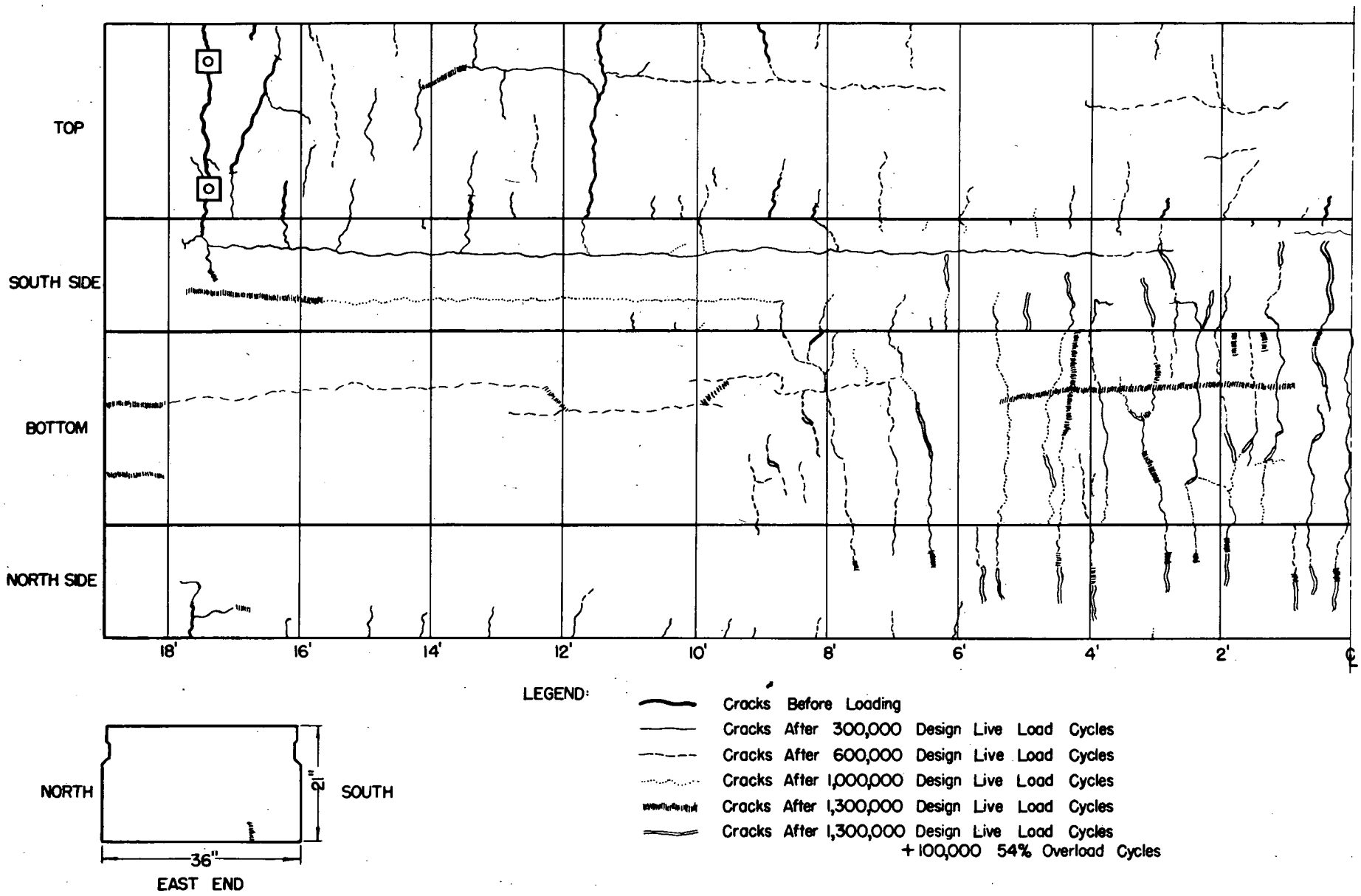

Fig. 26. DEVELOPED VIEW OF TEST BEAM SHOWING CRACKS
East Half of Beam

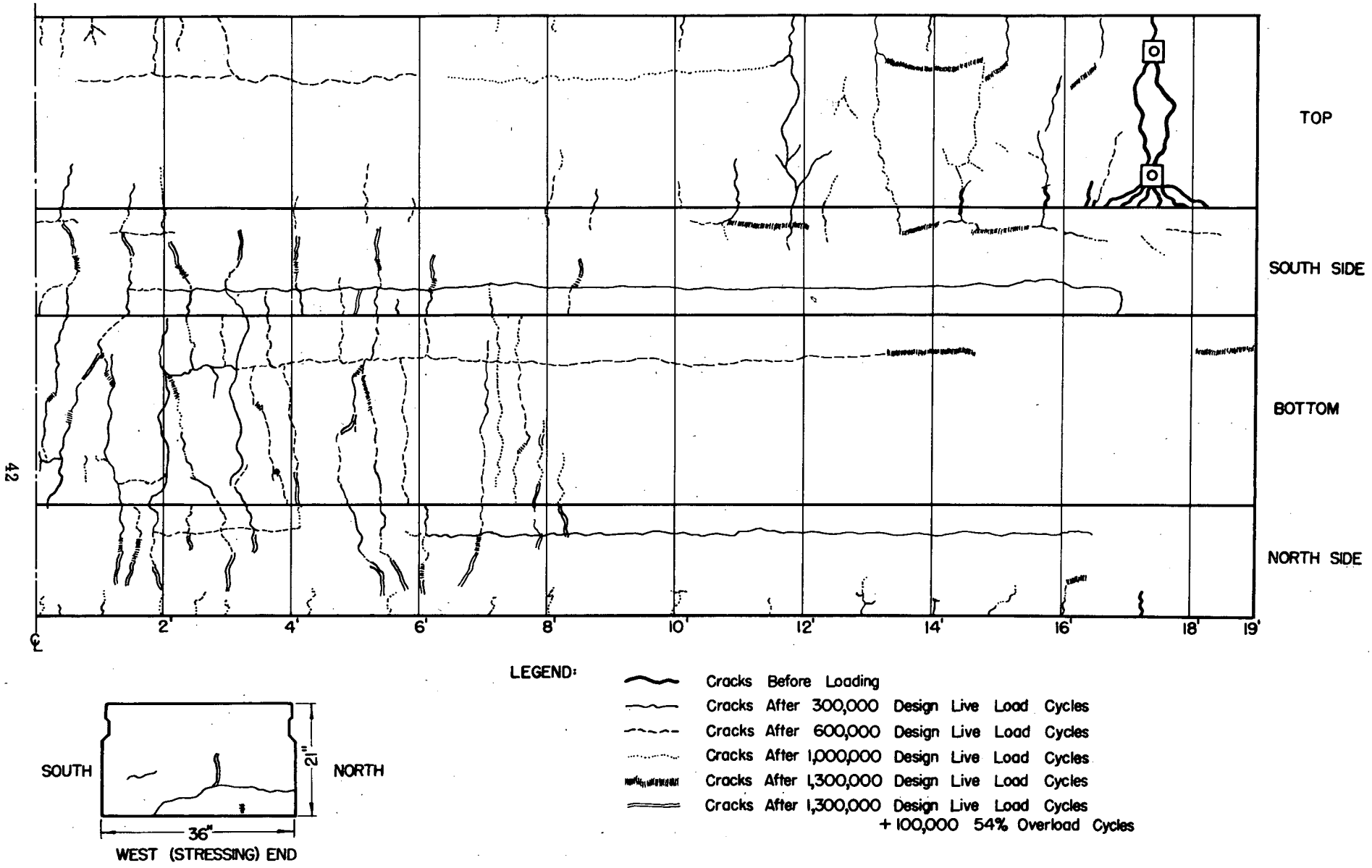

Fig. 27. DEVELOPED VIEW OF TEST BEAM SHOWING CRACKS
West Half of Beam

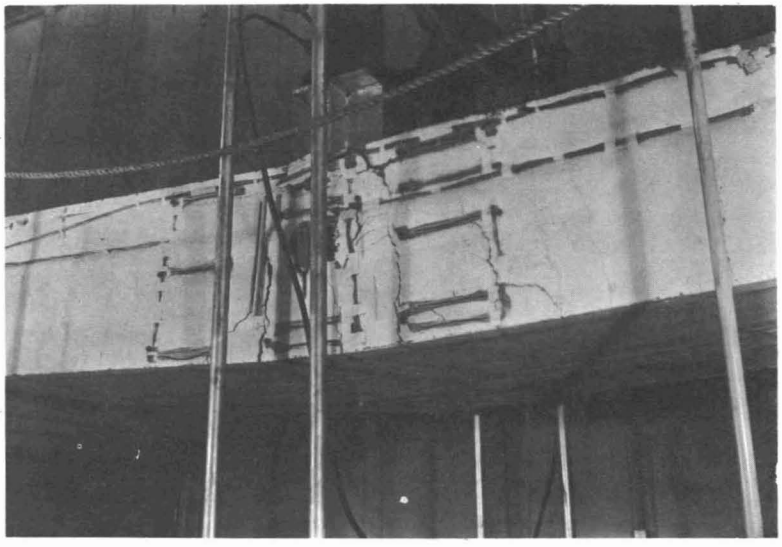

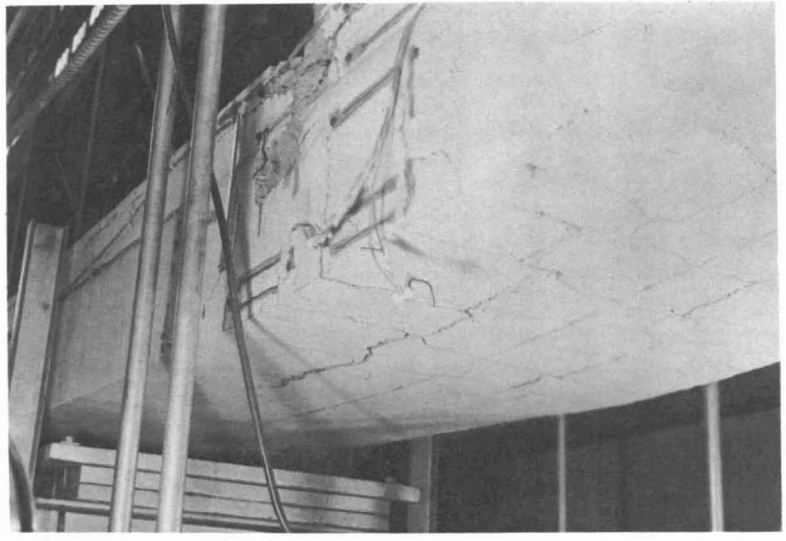

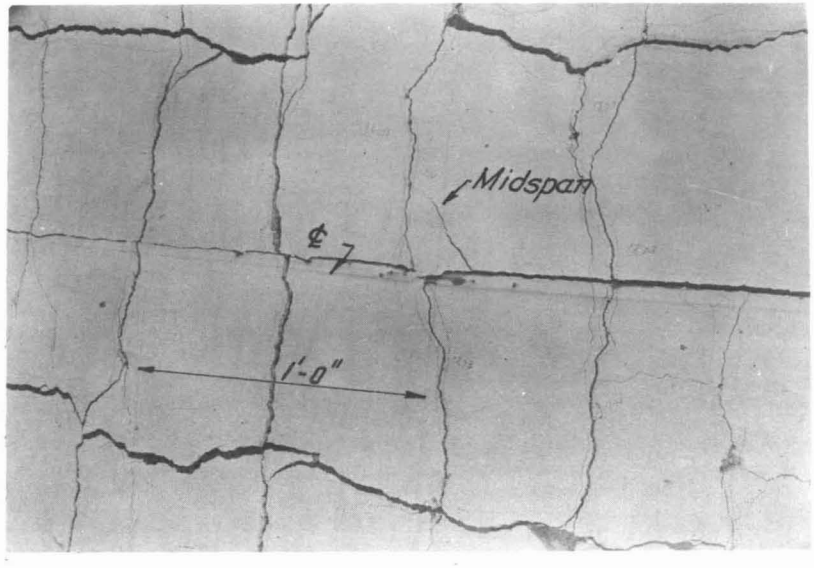

Fig. 28. SIDES OF BEAM AT CENTER AFTER FAILURE
Load 46,900 lbs., Deflection 13.7 in.

Fig. 29. BOTTOM FACE OF BEAM AT CENTER AFTER FAILURE
Load 46,900 lbs., Deflection 13.7 in.

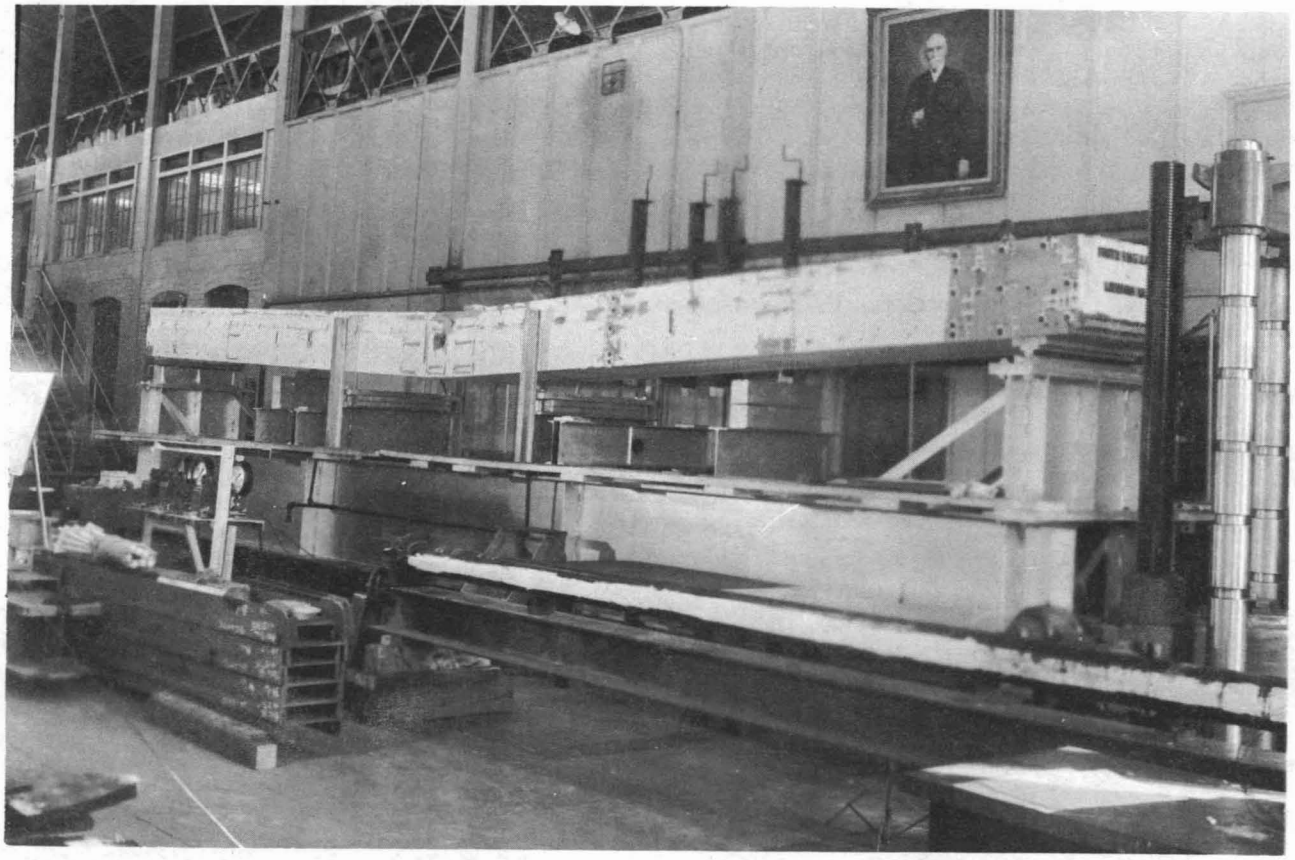

Fig. 30. TEST BEAM AFTER DESTRUCTION BY CENTER LOADING

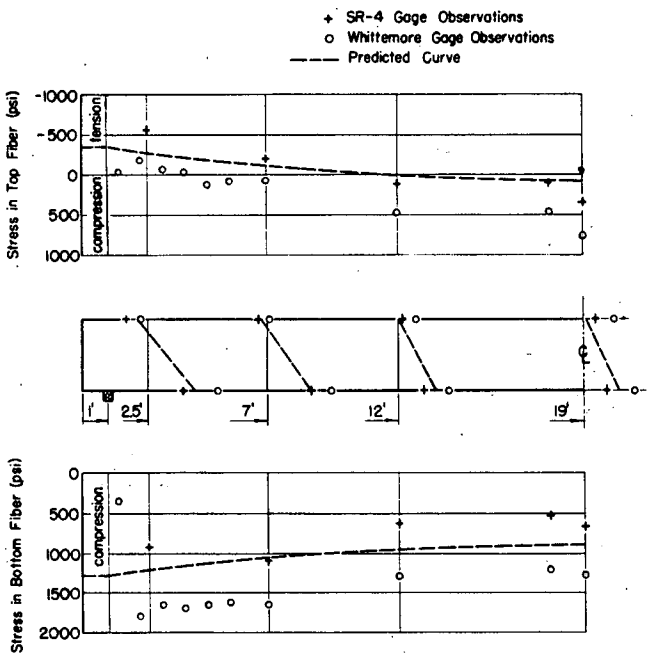

Fig. 31. CONCRETE BENDING STRESSES DUE TO INITIAL PRESTRESS AND DEAD LOAD

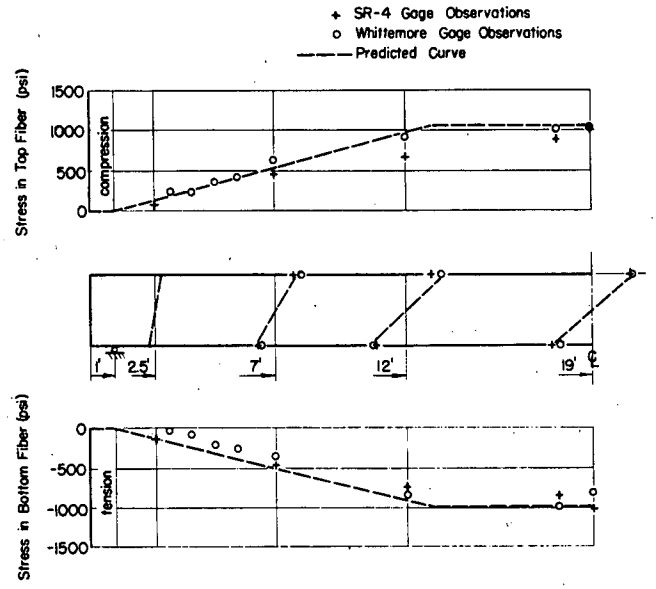

Fig. 32. CONCRETE BENDING STRESSES DUE TO DESIGN LIVE LOAD (1st. Static Test)

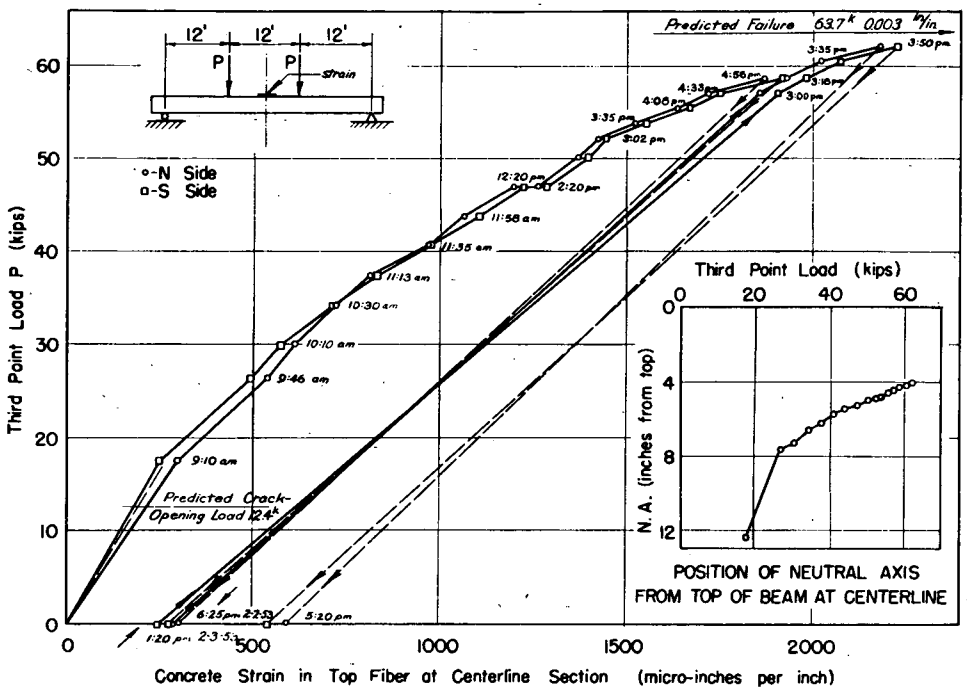

Fig. 34. STRAIN IN TOP CONCRETE FIBER DURING DESTRUCTION TEST

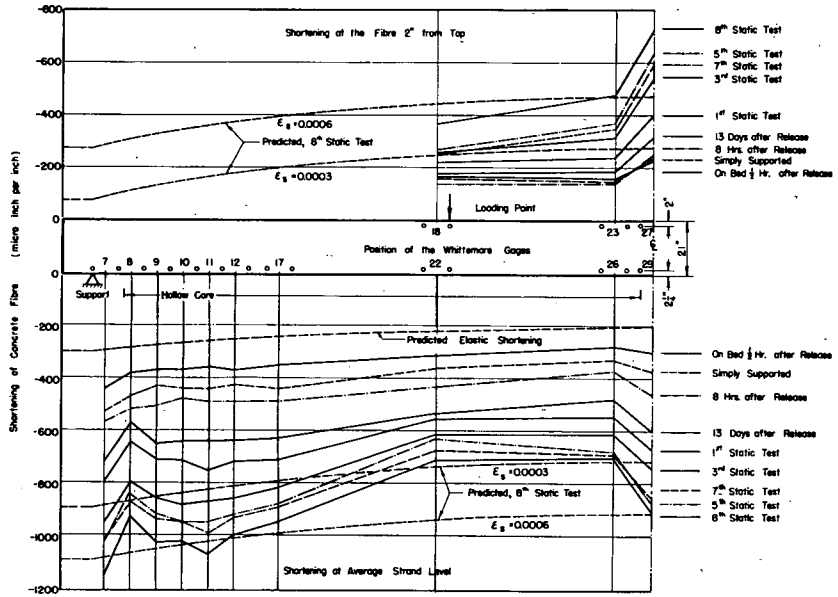

Fig. 35. CONCRETE FIBER SHORTENING ALONG BEAM

Fig. 33. CRACK-OPENING LOAD

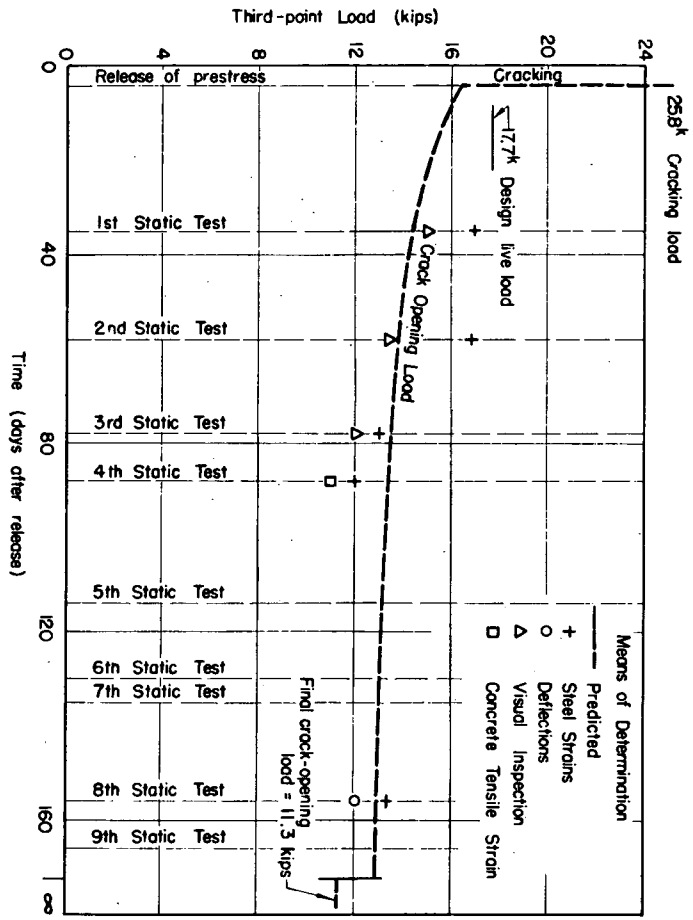

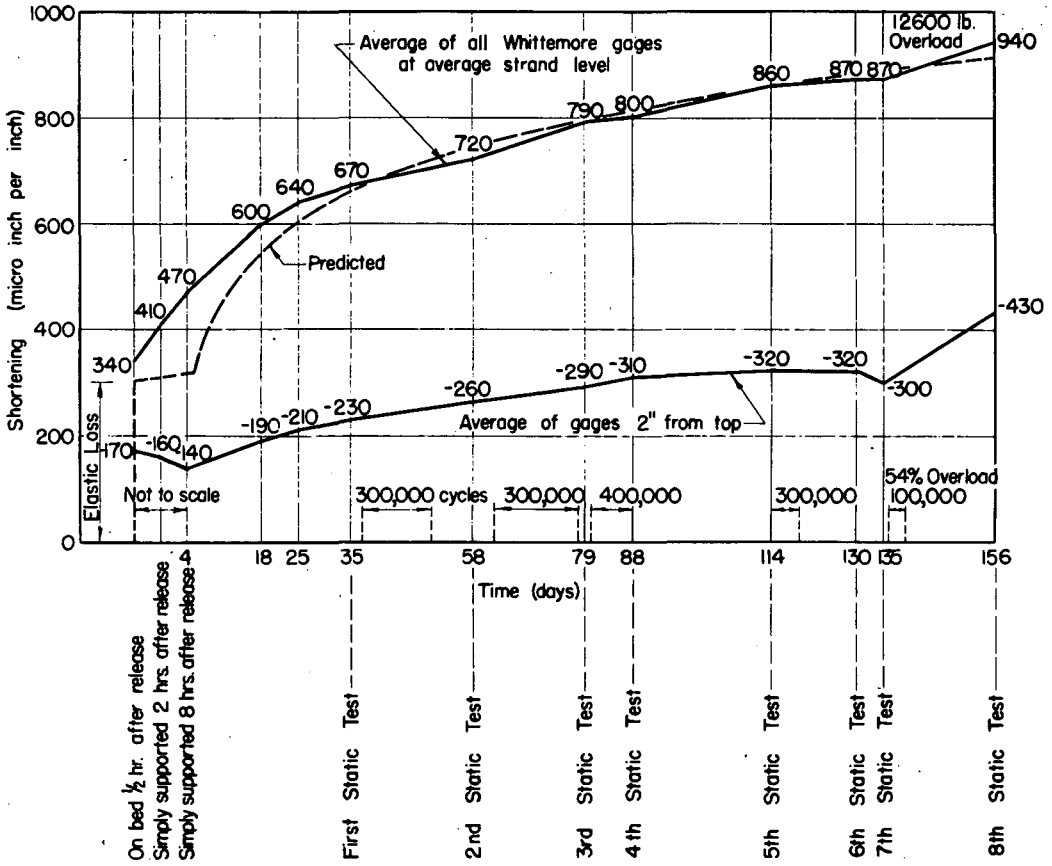

Fig. 36. CONCRETE FIBER SHORTENING
(Unloaded Beam)

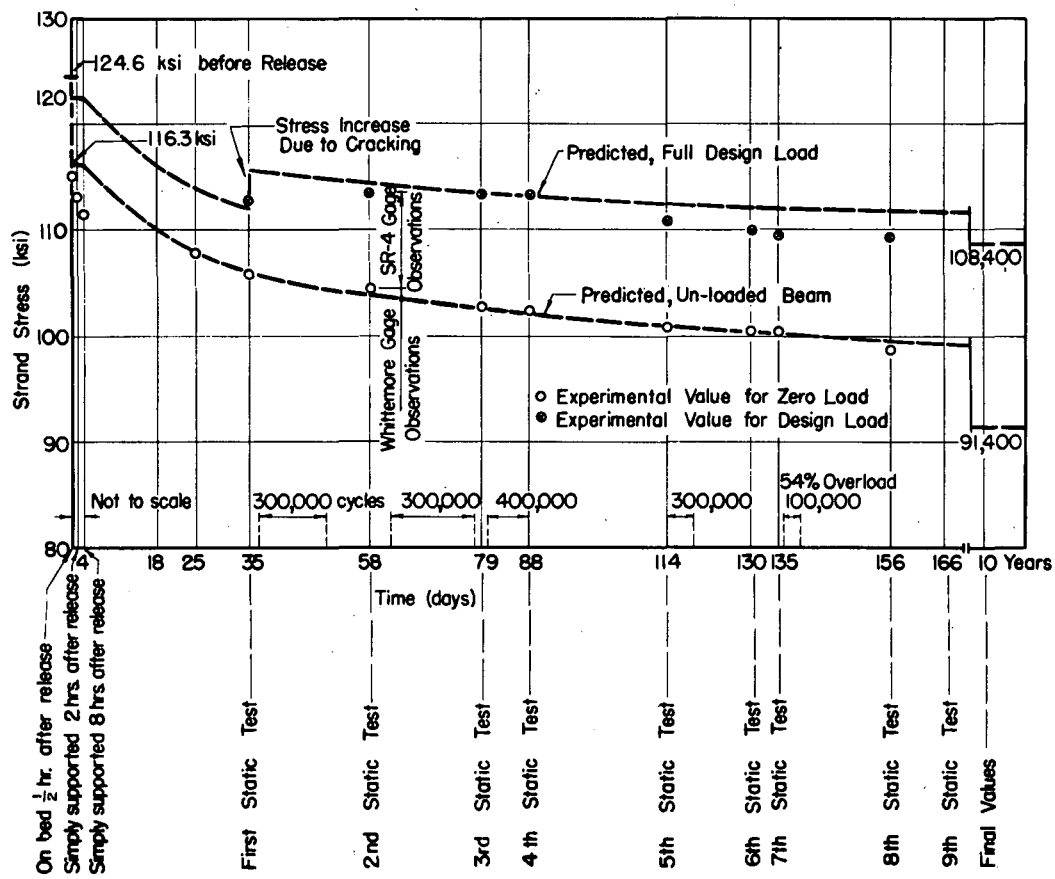

Fig. 37. CHANGE IN STRAND STRESS AT CENTER SECTION

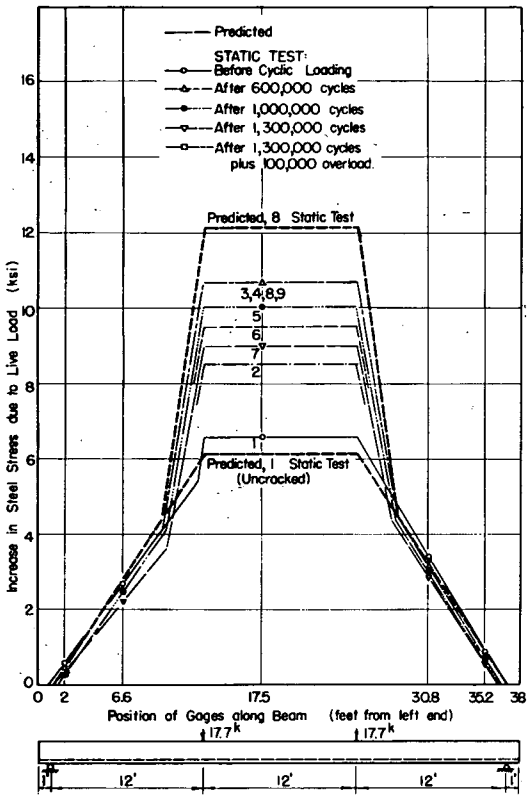

Fig. 38. DESIGN LIVE LOAD STEEL STRESSES ALONG BEAM

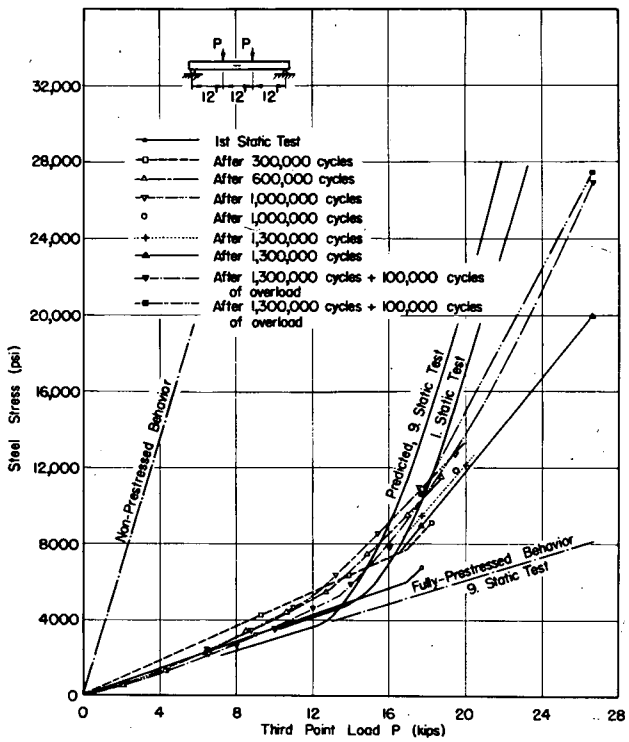

Fig. 39. INCREASE OF STEEL STRESS WITH LIVE LOAD

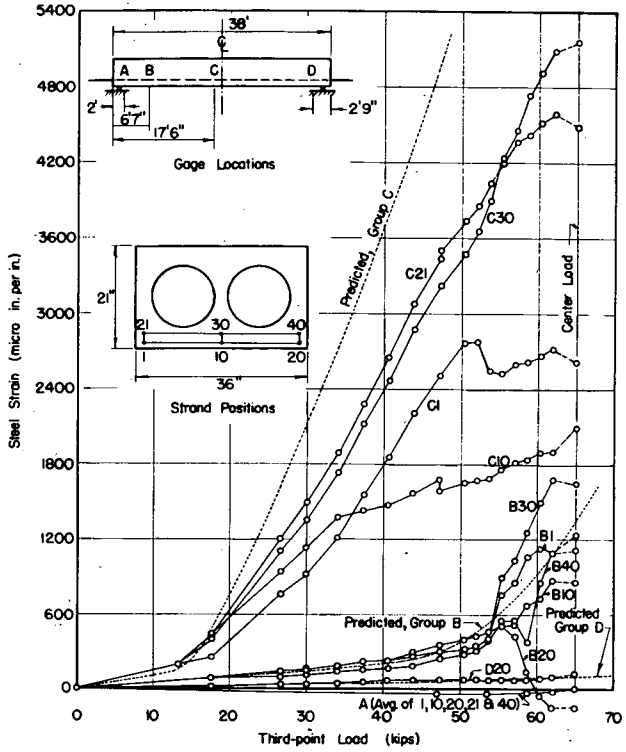

Fig. 40. LIVE LOAD STEEL STRAINS DURING DESTRUCTION TESTS

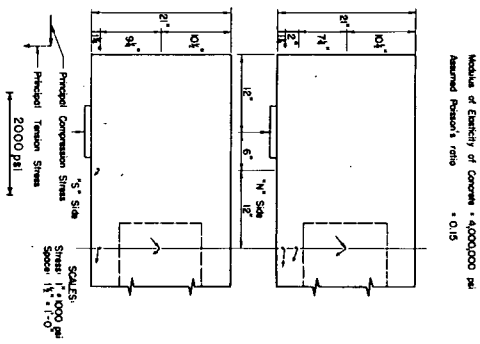

Fig. 42. PRINCIPAL STRESSES NEAR WEST END DUE TO DESTRUCTION LIVE LOAD

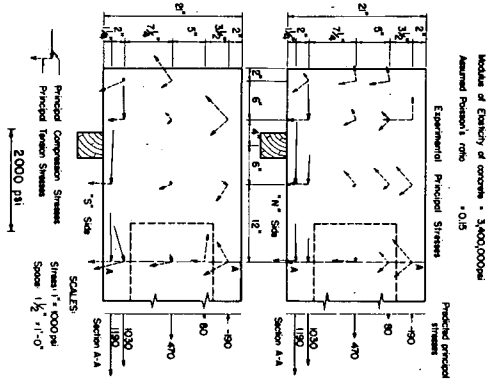

Fig. 41. PRINCIPAL STRESSES NEAR WEST END AT RELEASE OF STRANDS

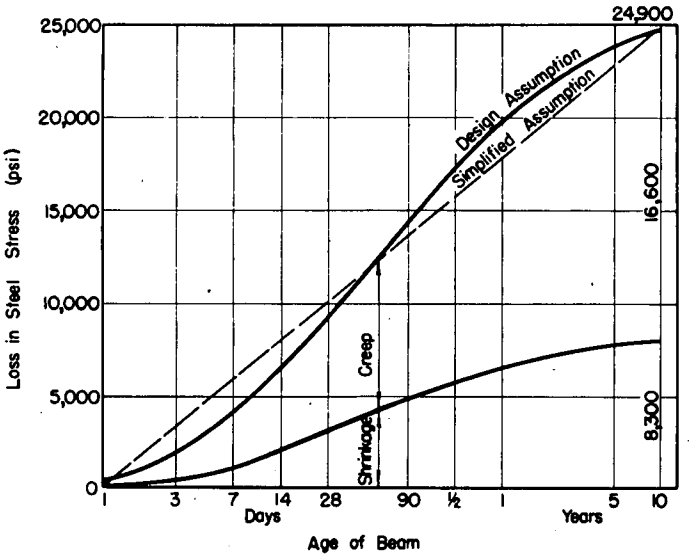

Fig. 43. ASSUMED LOSSES IN STRAND PRESTRESS Due to Progressive Creep and Shrinkage

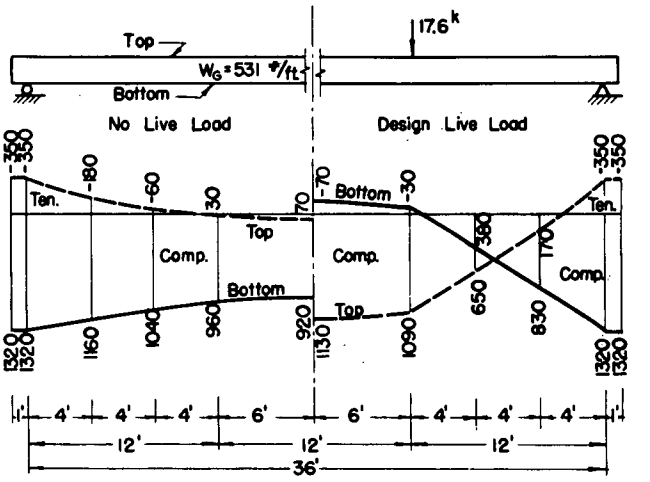

Fig. 44. DESIGN CONCRETE STRESSES BEFORE LOSSES

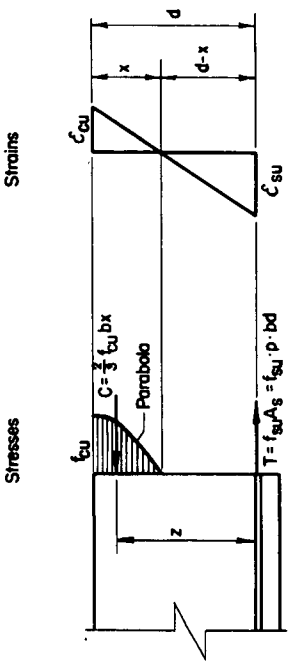

Fig. 45. STRESS AND STRAIN DISTRIBUTION AT FAILURE

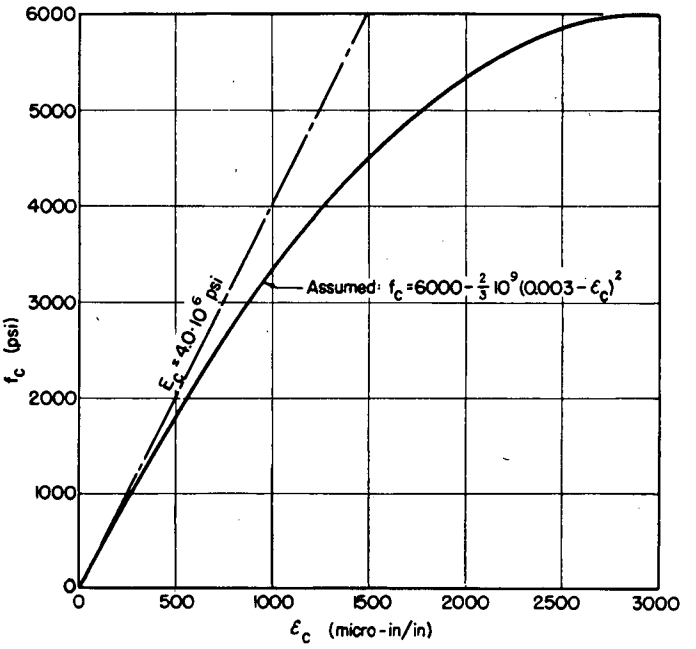

Fig. 46. CONCRETE STRESS-STRAIN DIAGRAM

K. Appendix

STRESS ANALYSIS OF PRETENSIONED 38 FT. TEST BEAM

1. Cross Section Properties

The cross section is shown in Fig. 1. Symbols used are explained in the nomenclature, p. 43,

E_c	=		3,750 ksi (average value, p. 15).
E_s	=		27,700 ksi (Fig. 18).
n	=	E_s/E_c	= 7.4
A_c	=		502 in^2
A_s	=		2.25 in^2
A'_c	=	$A_c + (n - 1) A_s$	= 516 in^2
c'_b	=		10.15 in.
c'_t	=		10.85 in.
I'_c		(hollow section)	= 26,000 in^4
I'_c		(solid section)	= 28,400 in^4
Q'_c		(hollow section)	= 1,770 in^3
Q'_c		(end block)	= 2,080 in^3
Z'_b	=	I'_c/c'_b	= 2,560 in^3
Z'_t	=	I'_c/c'_t	= 2,400 in^3
e'	=		7.90 in.
e'_l		(lower strand row)	= 8.90 in.
e'_u		(upper strand row)	= 6.90 in.
r'	=	$\sqrt{I'_c/A'_c}$	= 7.08 in.
p'	=	A_s/A'_c	= 0.00435
p	=	A_s/bd	= 0.00333
d	=		18.75 in.
b	=		36 in.

2. Design Load Moments and Shears

(2) Dead Load.

$$W_G = 502 \frac{150}{144} + 2.25 \frac{490}{144} = 531 \text{ lbs./ft.}$$

$$W_S = 3.30 = 90 \text{ lbs./ft. surfacing}$$

$$M_G = \frac{1}{8} \quad 531 \cdot 36^2 \cdot 12 = \underline{1{,}017{,}000 \text{ in. lbs.}}$$

$$M_S = \frac{1}{8} \quad 90 \cdot 36^2 \cdot 12 = 175{,}000 \text{ in. lbs.}$$

In the test M_s is produced by an additional third-point load P_s :

$$P_S = \frac{3M_S}{L} = \frac{3 \cdot 175{,}000}{36 \cdot 12} = 1220 \text{ lbs.} = V_S$$

$$V_G = 0.5 \cdot 531 \cdot 36 = \underline{9570 \text{ lbs.}}$$

(b) Live Load and Impact.

0.8 of the wheel load of H2O-S16-44 loading is carried by one beam. Moment and shears, see AASHO 1949 Spec. Pg. 241. Impact addition 30% (p. 7).

$$M_L = 0.5 \cdot 0.8 \cdot 378{,}900 \cdot 12 \cdot 1.30 = \underline{2{,}366{,}000 \text{ in. lbs.}}$$

Corresponding experimental third-point loading,

$$P_L = \frac{3M_L}{L} = \frac{3 \cdot 2{,}366{,}000}{36 \cdot 12} = 16{,}430 \text{ lbs.}$$

Total experimental third-point loading,

$$P = P_L + P_S = \underline{17{,}650 \text{ lbs.}} = V_L$$

3. Prestress

(a) Initial Strand Stress

Strands were each prestretched by 260 lbs., then elongated 4400 micro in/in according to SR-4 strain gage readings. ($E = 27.3 \times 10^6$ psi for swaged strand, see Fig. 18).

$$f_{si} = \frac{260}{0.0562} + (4400 \cdot 10^{-6})\ 27.3 \cdot 10^6 = 124{,}600 \text{ psi.}$$

The total measured elongation 6 5/8"over 120 ft length corresponds to 4600 micro in/in strain, part of which is assumed lost due to initial slack in the strands under the modest prestretch of only 260 lbs.

(b) Initial Prestress

Elastic loss in lower row of strands,

$$\Delta'_e = f_{si} - f_{so} = \frac{E_s}{E_c}\left(\frac{f_{so} \cdot A_s}{A'_c} + \frac{f_{se} A_s e' e'}{I'_c}\right)$$

$$= \left(f_{si} \quad \Delta'_e\right) n p' \left(1 + \frac{e' e'_i}{r'^2}\right)$$

$$= f_{si} \cdot \frac{np'\left(1 + \frac{e' e'_i}{r'^2}\right)}{1 + np'\left(1 + \frac{e' e'_i}{r'^2}\right)}$$

$$= 124{,}600 \cdot \frac{7.4 \cdot 0.00435\left(1 + \frac{7.90 \cdot 8.90}{7.08^2}\right)}{1 + 7.4 \cdot 0.00435\left(1 + \frac{7.90 \cdot 8.90}{7.08^2}\right)}$$

$= 9000$ psi or 7.2% of f_{si}

Δ^u_e = 7800 psi or 6.3% of f_{si}

f'_{so} = 124,600 - 9000 = 115,600 psi.

f^u_{so} = 124,600 - 7800 = 116,800 psi.

Except when considering the change in strand stress at release the average value Δ_e is sufficiently accurate:

$$\Delta_e = f_{si} \cdot \frac{np'\left(\frac{1 + e'^2}{r'^2}\right)}{1 + np'\left(\frac{1 + e'^2}{r'^2}\right)}$$

$= 8300$ psi or 6.7% of f_{si}

$f_{so} = 124{,}600 - 8300 = \underline{116{,}300 \text{ psi}}$

(c) Final Prestress

Shrinkage loss $\Delta_s = \epsilon_s \cdot E_s = 0.0003 \cdot 27.7 \cdot 10^6 =$ 8300 psi

Concrete creep loss $\Delta_p = 2 \cdot \Delta_e =$ 16,600 psi

Steel creep loss $\Delta_t =$ 0 psi

End anchorage deformation was measured to be 3/16" and was compensated for, 0 psi

Total loss in prestress (21% of f_{so}), $\Delta f_s =$ 24,900 psi

$f_{se} = f_{so} - \Delta f_s = 116{,}300 - 24{,}900 =$ 91,400 psi

The assumed rate of loss of prestress is shown in Fig. 43 based on studies at EMPA, Zürich, Switzerland.

4. Design Load Stress

(a) Concrete Bending Stresses.

Prestress:

$$f^b_{F_o} = F_o\left(\frac{1}{A'_c} + \frac{e'}{Z'_b}\right) + = 116{,}300 \cdot 2.25\left(\frac{1}{516} + \frac{7.90}{2560}\right) = 1315 \text{ psi.}$$

$$f^t_{F_o} = F_o\left(\frac{1}{A'_c} - \frac{e'}{Z'_t}\right) = 261{,}700\left(\frac{1}{516} - \frac{7.90}{2400}\right) = -354 \text{ psi.}$$

Subsequent losses (Fig. 43) reduce these stresses as follows:

CONCRETE STRESSES AT MIDSPAN DUE TO PRESTRESS ONLY

Static Test No.	Days After Casting	Prestress Loss In Steel		f^b_F	f^t_F
		psi	%	psi	psi
0	0	0	0	1315	-354
1	35	10,400	8.6	1197	-323
2	58	12,500	10.8	1174	-316
3	79	13,800	11.9	1159	-312
4	88	14,200	12.2	1154	-311
5	114	15,300	13.2	1142	-308
6	130	16,000	13.8	1134	-306
7	135	16,200	13.9	1132	-305
8	156	16,800	14.4	1125	-303
9	166	17,000	14.6	1122	-303
Final Value	10 years	24,900	21.4	1033	-278

Dead Load:

$$f^b_G = -\frac{M_G}{Z'_b} + = -\frac{1{,}017{,}000}{2560} = -397 \text{ psi.}$$

$$f_G^t = \frac{Mc}{Z_t'} = \frac{1{,}017{,}000}{2400} = 423 \text{ psi.}$$

Live Load, Impact, and Surfacing:

$$f_L^b = -\frac{M_L + M_S}{Z_b'} = -\frac{2{,}366{,}000 + 175{,}000}{2560} = -993 \text{ psi.}$$

$$f_L^t = \frac{M_L + M_s}{Z_t'} \quad -\frac{2{,}541{,}000}{2400} = 1060 \text{ psi}$$

Combined Stresses At Beam Center Before (After) Losses (psi):

Prestress	Dead Load		Live Load	Combined Stresses
-354 (-278)	423	69 (145)	1060	1129 (1205)

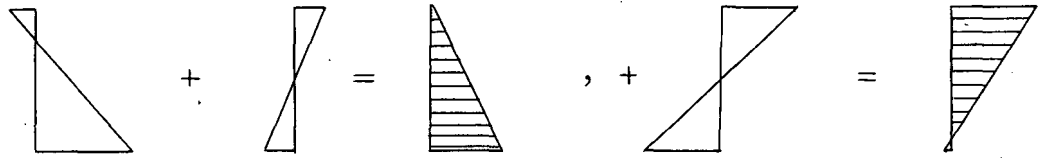

1315 (1033)	-397	918 (636)	-993	-75 (-357)
F_o	G	$F_o + G$	L	$F_o + G + L$

COMBINED CONCRETE STRESSES AT MIDSPAN DURING TEST PERIOD (psi):

STATIC TEST NO.	DAYS AFTER CASTING	PRESTRESS & DEAD LOAD		FULL DESIGN LOAD (*)	
		Bottom	Top	Bottom	Top
0	0	918	69	-75	1129
1	35	800	100	-193	1160
2	58	777	107	-216	1167
3	79	762	111	-231	1171
4	88	757	112	-236	1172
5	114	745	115	-248	1175
6	130	737	117	-256	1177
7	135	735	118	-258	1178
8	156	728	120	-265	1180
9	166	725	120	-268	1180
Final Yalue	10 years	636	145	-357	1205

(*) Prestress + Dead Load + Live Load + Impact

The stress distribution along the top and bottom fibers of the beam at the time of release of prestress is shown in Fig. 44.

(b) Steel Stresses

Assuming un-cracked section and no internal bond failure the change in steel stress is n times the change in stress in the surrounding concrete.

Bottom Fiber $c_b' = 10.15$ in.

Lower Strand Row $e_l' = 8.90$ in.

Upper Strand Row $e_u' = 6.90$ in.

$$f_s' = n\frac{e_l'}{c_b'} \cdot f_c^b = 7.4\frac{8.90}{10.15} \cdot f_c^b = 6.48 \cdot f_c^b$$

$$f_s^u = n\frac{e_u'}{c_b'} \cdot f_c^b = 7.4\frac{6.90}{10.15} \cdot f_c^b = 5.03 \cdot f_c^b$$

$$f_s^{ave} = n \frac{e'}{c'_b} \cdot f_c^b = 7.4 \frac{7.90}{10.15} \cdot f_c^b = 5.77 \cdot f_c^b$$

The calculated change in bending stresses in the concrete and in the strands due to the simultaneous application of prestress and dead weight and due to design live load are shown below for various locations along the beam. The n-value used above is the average value for the duration of the test. The more accurate incidental n-values are used in some places where required for accuracy.

Change in Bending Stresses (psi), due to release of prestress ($F_O + G$), and due to live load (17,650 lbs. at third-points):

Distance from Support (ft.)	CONCRETE				STEEL			
	Bottom		Top		Lower		Upper	
	Release	L. L.	Release	L. L.	Release	L. L.	Release	L. L.
0	1320	0	-350	0	-9000	0	-7800	0
4	1160	-330	-180	350	-8000	2100	-7000	1700
8	1040	-660	- 60	710	-7200	4300	-6400	3300
12	960	-990	30	1060	-6700	6400	-6000	5000
18	920	-990	70	1060	-6400	6400	-5800	5000

Steel stresses due to design live load after cracking, see p. 77.

(c) Diagonal Tension Stresses.

Shear stress (conventionally computed) due to dead weight at c.g.c', in end block:

$$v = \frac{V_G \; Q'_c}{I'_c \; b} = \frac{9570 \cdot 2080}{28{,}400 \cdot 36} = 19 \text{ psi},$$

at start of cored section:

$$v = \frac{9040 \cdot 1770}{26{,}000 \cdot 11} = 56 \text{ psi}.$$

The effect of these shear stresses on the principal stresses is negligible in comparison with the prestress.

Shear stresses due to full experimental design load at c.g.c', in solid end block:

$$v = \frac{(V_G + V_L) \; Q'_c}{I'_c \quad b} = \frac{(9570 + 17{,}650)\; 2080}{28{,}400 \cdot 36} = 55 \text{ psi},$$

at start of cored section:

$$v = \frac{(9040 + 17{,}650)\; 1770}{26{,}000 \cdot 11} = \underline{165 \text{ psi}}.$$

The actual H20-S16 loading, at the start of the cored section, causes:

$$v = \frac{(V_G + V_S + V_L)\, Q'_c}{I'_c \cdot b} = \frac{(9040 + 1530 + 26{,}700)\; 1770}{26{,}000 \cdot 11} = 231 \text{ psi}.$$

Maximum principal stresses due to full experimental design load will occur at the start of the cored section and very near the c.g.c'.

$$\left.\begin{matrix} S_c \\ S_t \end{matrix}\right\} = \frac{S_x}{2} \pm \sqrt{\frac{S_x^2}{4} + v^2} = \frac{507}{2} \pm \sqrt{253^2 + 165^2} = \begin{cases} 560 \text{ psi}. \\ \underline{-50 \text{ psi}}. \end{cases}$$

Similarily, the actual H2O-S16 loading causes;

$$\left.\begin{matrix} S_c \\ S_t \end{matrix}\right\} = \frac{507}{2} \pm \sqrt{253^2 + 231^2} = \begin{cases} 600 \text{ psi}. \\ -90 \text{ psi}. \end{cases}$$

Thus the experimental loading, giving the same maximum moments as the H20-S16 loading, causes smaller shear and diagonal tension stresses.

5. Cracking Load

(a) First Cracking Load:

At age 35 days, first application of live load,

f'_c = 5000 psi. (p. 15).

$R = 10\sqrt{f'_c}$ = 700 psi, or

$R = 0.13 \cdot f'_c$ = 650 psi. Use the smaller value.

Stress at midspan due to prestress at 35 days (see p. 73),

f^b_F = 1200 psi.

The addition of dead weight causes (p. 74).

f^b_{FG} = 800 psi

Live load alone gives

f^b_L = -990 psi.

Multiple m of live load causing cracking,

$$m = \frac{f_{FG}{}^b + R}{f^b_L} \quad \frac{800 + 650}{990} = \underline{1.5}$$

Multiple m' of dead + live load causing cracking,

$$m' = \frac{f_F{}^b + R}{f_{G}{}^b + f_L{}^b} = \frac{1200 + 650}{400 + 990} = \underline{1.3}$$

(b) Crack Opening Load

After cracking has once taken place the cracks will open when the bottom fiber compressive stress is reduced to zero through application of live load:

$f^b_{FT} = f^b_{FG} + f^b_L = 0$

Thus, the crack-opening load is:

STATIC TEST No.	$f^b_{FG} = -f^b_L$ (psi)	CRACK OPENING LOAD	
		Part of Design L. L. %	Third-point Load pounds
0	918	93	16,320
1	800	81	14,220
2	777	78	13,810
3	762	77	13,540
4	757	76	13,460
5	745	75	13,240
6	737	74	13,100
7	735	74	13,060
8	728	73	12,940
9	725	73	12,890
Final Value	636	64	11,300

The additional steel stress f_{sb} in a cracked section over and above the live load steel stress at crack-opening load may be computed in several ways:

(a) Accurately, considering the shift of the neutral axis with increasing load consistent with the straight-line strain distribution.

(b) Approximately, assuming $A_s \cdot f_{sb}$ to equal the tension in the concrete as computed assuming a homogeneous section.

(c) Approximately, as a regular reinforced section.

Method (a) is very cumbersome, especially when the cross-section width b varies with the depth. Method (b) gives somewhat too high values for f_{sb} but is very simple and is used in the German tentative specifications DIN 4227. Method (c) gives even larger values, without being easier in use.

f_{sb} is calculated below by method (b). The distance c is the length of the cracks from the bottom fiber assumed equal to distance to neutral exis from the bottom fiber. For comparison, the steel stress due live load were there no prestress present is computed as for a normally reinforced section:

$$f_{sL} = \frac{M_L}{A_s z}, \text{ where}$$

$$z = d - \frac{d}{3} np \left(-1 + \sqrt{1 + \frac{2}{np}} \right).$$

STEEL STRESS DUE TO LIVE LOAD, CRACKED SECTION

Static Test No.	f^b_{FT} (psi) Homogeneous Section	Crack Length (x) c (in)	f_s at crack opening load (psi)	$f_{sb} = \frac{bc}{2A_s} f^b_{FT}$ (psi)	f_{sL} (psi)
1 (uncracked)	-193	0	6120	0	6120
1 (cracked)	-193	3.00	4830	4630	9460
2	-216	3.28	4650	5680	10,330
3	-231	3.46	4440	6390	10,830
4	-236	3.52	4350	6650	11,000
5	-248	3.66	4210	7260	11,470
6	-256	3.75	4050	7680	11,730
7	-258	3.78	4030	7800	11,830
8	-265	3.85	3970	8160	12,130
9	-268	3.89	2900	8340	12,240
Final Value	-357	4.80	3270	13,700	16,970
No Prestress					64,500

(x) Distance to neutral axis from bottom fiber

6. Ultimate Load

(a) Bending

The following method for predicting the ultimate moment of the section is based on the assumption that plane sections remain plane up to the ultimate load, that the ultimate steel stress is above the "yield" level (0.2% permanent set) thus allowing sufficient elongation to cause compression failure of the concrete, and that the concrete stress-strain diagram is parabolic up to the ultimate stress f_{cu} (Fig. 46).

From the linear strain distribution (Fig. 45) follows:

$$\frac{\varepsilon_{cu}}{\varepsilon_{su}} = \frac{x}{d-x}$$

Equilibrium between steel tension T and concrete compression C gives:

$$f_{su}\ p\ bd\ \frac{2}{3}\ f_{cu}\ bx$$

These two equations yield

$$z = \frac{3}{2}\frac{f_{su}}{f_{cu}}\ pd \qquad (1)$$

$$p = \frac{2}{3}\frac{f_{su}}{f_{su}}\ \frac{\varepsilon_{cu}}{\varepsilon_{cu} + \varepsilon_{su}} \qquad (2)$$

The assumed parabolic concrete stress-strain diagram (Fig. 46) result in

$$\varepsilon_{cu} = \varepsilon'_c = \frac{2f'_c}{E_c} = \frac{2 \cdot 6000}{4.00 \cdot 10^6} = 0.30\%$$

The stress in the top concrete fiber due to prestress and dead load is small (120 psi) and the corresponding strain (0.003%) is negligible.

Steel and concrete fail simultaneously if also $\varepsilon_{su} = \varepsilon'_s = 4\%$, of which $\frac{f_{se}}{E_s} = \frac{99{,}300}{27{,}700{,}000} =$ 0.36% is absorbed in prestress.

From Eq. (2), then, simultaneous steel and concrete failure would occur for

$$p_s = \frac{2}{3} \frac{6{,}000}{275{,}000} \frac{0.30}{0.30 + (4.00 - 0.36)} = 0.11\%$$

The upper limit for under-reinforced design is

$$p_b = \frac{2}{3} \frac{6{,}000}{240{,}000} \frac{0.30}{0.30 + (0.97 - 0.36)} = 0.55\%$$

With an actual p = 0.33% the steel stress at ultimate moment is less than $f'_s = 275{,}000$ psi but above the "yield" stress $f_{0.2} = 240{,}000$ psi. By trial it is found that $f_{su} = 263{,}000$ psi, which according to the steel stress-strain diagram (extrapolated on Fig. 18) corresponds to $\varepsilon_{su} = 1.45\%$, gives

$$p = \frac{2}{3} \frac{6{,}000}{263{,}000} \frac{0.30}{0.30 + (1.45 - 0.36)} = 0.33\%$$

which checks with the actual value of p and thus satisfies the assumption of linear strain distribution.

From Eq. (1) then,

$$x = \frac{3}{2} \frac{263{,}000}{6000} 0.0033 \cdot 18.75 = 4.07 \text{ in.}$$

From Fig. 45:

$z = d - \frac{3}{8} x = 18.75 - 0.375 \cdot 4.07 = 17.23$ in.

$M_u = f_s \cdot A \cdot z = 263{,}000 \cdot 2.25 \cdot 17.23 = 10{,}200{,}000$ in. lbs.

The dead weight moment absorbs 1,192,000 in. lbs.

The ultimate live load moment M_{uL} = 9,008,000 in. lbs.

corresponding to $M_D + 3.8 \cdot M_L$

or $2.9 (M_D + M_L)$

(b) Diagonal Tension Stress

End shear $V_L = \frac{3M_{uL}}{L} = \frac{9{,}008{,}000}{114} = 62{,}500$ lbs.

V_S (p.71) = 1,220 lbs.

V_G (p.71) = 9,570 lbs.

V = 73,290 lbs.

$$v = \frac{VQ}{I'_c b} = \frac{73{,}290 \cdot 1770}{26{,}000 \cdot 11} = 450 \text{ psi.}$$

Normal stress due to prestress,

$$f_F = \frac{0.854 \cdot 116{,}300 \cdot 2.25}{516} = 432 \text{ psi.}$$

Diagonal tension at predicted ultimate load,

$$S_t = \frac{432}{2} - \sqrt{216^2 + 450^2} = -285 \text{ psi.}$$

7. Deflections

(a) Working Load:

Centerline deflection of a simply supported beam subjected to equal third-point loads:

$$\delta_{L/2} = \frac{23}{648}\,\frac{PL^3}{E_c I_c'} = \frac{23}{648}\,\frac{17{,}650 \cdot 432^3}{E_c \cdot 26{,}000} = \frac{1940 \text{ kip/in}}{E_c}$$

Deflection at the quarter points:

$$\delta_{L/4} = \frac{29}{1152} \cdot \frac{PL^3}{E_c I_c'} = \frac{1380 \text{ kip/in}}{E_c}$$

Using the concrete cylinder test values of E_c (p. 15) the predicted centerline and quarter-point deflections are:

Static Test No.	E_c (ksi)	$\delta_{L/2}$ (in)	$\delta_{L/4}$ (in)
1	3500	0.55	0.39
2	3600	0.54	0.38
3	3700	0.53	0.37
4	3750	0.52	0.37
9	4000	0.49	0.35

(b) Ultimate Load:

The moment of inertia of the cracked section at ultimate moment, x = 4.07 in., is

$$I = 4400 \text{ in}^4$$

Assuming the moment of inertia to vary linearly from I_c' at the support to I at the third-point the ultimate deflection is

$$\delta_u = \frac{5}{72}\,\frac{M_{uL} L^2}{E_c I} + \int_0^{L/3} \frac{3M_{uL} \cdot x^2}{E_c I_c' L - 3E_c (I_c' - I)\, x}\, dx$$

An approximate numerical integration gives

$$\delta_u = 6.78 + 2.62 = 9.4 \text{ in.}$$

8. Summary of Design and Allowable Stresses

	Design Stresses	Allowable Stresses (Pa. Dept. of Hwys., 1/1/53 recommendation)	
(a) Steel			
f_s'	275,000 psi		200,000 psi min.
$f_{0.2}$	240,000 psi	$0.70\, f_s'$	= 193,000 psi min.
f_{si}	124,600 psi	$0.60\, f_s'$	= 165,000 psi max.
		$0.80\, f_{0.2}$	= (192,000 psi max.)
Δf_s	24,900 psi	$0.20\, f_{so}$	= 23,300 psi min.
(b) Concrete			
f_c'	5,000 psi		5,000 psi min.
f_{ci}'	3,300 psi	$0.67\, f_c'$	= 3,300 psi min.
f_c	1,210 psi	$0.35\, f_c'$	= 1,750 psi max.
f_{ci}	1,320 psi	$0.30\, f_c'$	= 1,500 psi max.
f_t^b	-360 psi	$-0.03\, f_c'$	= -150 psi max.
f_t^t	-350 psi	$-0.08\, f_c'$	= -400 psi max.
v	165 psi	$0.04\, f_c'$	= 200 psi max.
S_t	-50 psi	$0.04\, f_c'$	= -200 psi max.
S_{tu}	-285 psi	$-0.065\, f_c'$	-325 psi max.

M_{crack} $\quad M_D + 1.5 M_L$ / $1.3 (M_D + M_L)$ $\quad 1.5 (M_D + M_L)$ $= 445$ k. ft.

M_{ult} $\quad M_D + 3.8 M_L$ / $2.9 (M_D + M_L)$ $\quad 2.5(M_D + M_L)$ $= 741$ k. ft.

(c) Deflection

$\delta_{L/2}$ $\quad 0.52$ in. $\quad \left(\frac{L}{800} \right.$ $= 0.54$ in.)